A comprehensive sensitivity and uncertainty analysis for discharge and nitrate-nitrogen loads involving multiple discrete model inputs under future changing conditions

Christoph Schürz[1], Brigitta Hollosi[2], Christoph Matulla[2], Alexander Pressl[3], Thomas Ertl[3], Karsten Schulz[1], and Bano Mehdi[1,4]

[1]Institute of Water Management, Hydrology and Hydraulic Engineering, University of Natural Resources and Life Sciences, Vienna (BOKU), Vienna, Austria
[2]Department of Climate Research, Zentralanstalt für Meteorologie und Geodynamik (ZAMG), Vienna, Austria
[3]Institute of Sanitary Engineering and Water Pollution Control, University of Natural Resources and Life Sciences, Vienna (BOKU), Vienna, Austria
[4]Division of Agronomy, Department of Crop Sciences, University of Natural Resources and Life Sciences, Vienna (BOKU), Tulln, Austria

Correspondence: Christoph Schürz (christoph.schuerz@boku.ac.at)

Abstract. Environmental modeling studies aim to infer the impacts on environmental variables that are caused by natural and human-induced changes in environmental systems. Changes in environmental systems are typically implemented as discrete scenarios in environmental models to simulate environmental variables under changing conditions. The scenario development of a model input usually involves several data sources and perhaps other models, that are potential sources of uncertainty. The

5   setup and the parametrization of the implemented environmental model are additional sources of uncertainty for the simulation of environmental variables. Yet, to draw well-informed conclusions from the model simulations it is essential to identify the dominant sources of uncertainty.

In impact studies in two Austrian catchments the eco-hydrological model Soil and Water Assessment Tool (SWAT) was applied to simulate discharge and nitrate-nitrogen (NO_3^--N) loads under future changing conditions. For both catchments the

10   SWAT model was set up with different spatial aggregations. Non-unique model parameter sets were identified that adequately reproduced observations of discharge and NO_3^--N loads. We developed scenarios of future changes for land use, point source emissions, and climate and implemented the scenario realizations in the different SWAT model setups with different model parametrizations, which resulted in 7000 combinations of scenarios and model setups for both catchments. With all model combinations we simulated daily discharge and NO_3^--N loads at the catchment outlets.

15   The analysis of the 7000 generated model combinations of both case studies had two main goals; i) to identify the dominant controls on the simulation of discharge and NO_3^--N loads in the two case studies, and ii) to assess how the considered inputs control the simulation of discharge and NO_3^--N loads. To assess the impact of the input scenarios, the model setup and the parametrization on the simulation of discharge and NO_3^--N loads we employed methods of global sensitivity analysis (GSA). The uncertainties in the simulation of discharge and NO_3^--N loads that resulted from the 7000 SWAT model combinations

were evaluated visually. We present approaches for the visualization of the simulation uncertainties that proved to support the diagnosis of how the analyzed inputs affected the simulation of discharge and NO_3^--N loads.

Based on the GSA we identified climate change and the model parametrization to be the most influential model inputs for the simulation of discharge and NO_3^--N loads in both case studies. In contrast, the impact of the model setup on the simulation of discharge and NO_3^--N loads was low and the changes in land use and point source emissions were found to have the lowest impact on the simulated discharge and NO_3^--N loads. The visual analysis of the uncertainty bands illustrated that the anomalies in precipitation of the different climate scenarios dominated the changes in simulation outputs, while the differences in air temperature showed no considerable impact.

1 Introduction

Environmental systems are under constant change. Predicting the development of natural resources in a changing system involves large uncertainties (Milly et al., 2008). Climate change, in concurrence with other dynamic processes such as population growth, land use change or economic development pose challenges to the management of water supply and water quality (Duran-Encalada et al., 2017; Yates et al., 2015). Human disturbances can exacerbate the impacts of climate and amplify consequences to water quality (Jiménez et al., 2014) on one hand. On the other hand, stakeholders in environmental systems have to respond to future changes, for instance adapting farm management practices due to changes in temperatures and precipitation patterns (Schönhart et al., 2018). Ideally, an impact assessment considers all future changes that can affect the development of the environment of interest as well as those future changes that can introduce uncertainties in the simulation of the environmental variables of interest.

Changes in environmental systems are typically represented by discrete scenarios in impact studies. Preferably, the set of scenarios representing a dynamic change covers the full range of trajectories along which the development is plausible (Clark et al., 2016). Scenario development involves different data sources and models, which can introduce and propagate uncertainties. For example, climate scenarios have several sources of uncertainty and may include several socioeconomic scenarios (e.g. the current "Representative Concentration Pathways" (RCP; Moss et al., 2010; van Vuuren et al., 2011)) that drive an array of global climate models (GCM) (Knutti and Sedláček, 2013). However, the GCMs also have inherent uncertainty and they provide the boundary conditions for regional climate models (RCM) (e.g. Jacob et al., 2014). Further, the downscaling (Wilby et al., 1998; Wood et al., 2004) of the RCM simulations and the bias correction (Teutschbein and Seibert, 2013, 2012) are associated with their own uncertainty and are a standard procedures in climate scenario development. Eventually, it is essential to characterize the uncertainties inherent in all processes that affect the simulation of an environmental variable.

To simulate the development of hydrological variables under changing conditions, the developed scenarios are implemented as boundary conditions in hydrological models that are calibrated for historic observations. Yet, often different model setups and different sets of parameters in a model can perform equally well to reproduce historical observations of the variables of interest. Equifinality is a well-known issue in hydrologic modeling that has been extensively addressed in the literature (e.g. Schulz et al., 1999; Beven, 2006; Beven and Freer, 2001; Beven, 1996), where multiple model structures (e.g. Clark et al.,

2008) and model parametrizations (e.g. Schulz et al., 1999) represent observations equally well and thus cannot be rejected (Beven, 2006). An adequate representation of historical data does not necessarily assure that different model setups agree when extrapolating to future conditions (Chiew and Vaze, 2015; Milly et al., 2008). Thus, differences in the model setup are a source of uncertainty in the simulation of an environmental variable under future conditions.

5   Altogether, an impact study comprises an abundance of combinations of trajectories of system changes and model setups to describe an environmental system that ultimately characterize the uncertainties in a simulation. Hence, a comprehensive description of the uncertainties in model simulations is a major challenge of any impact study.

Model sensitivity analysis (SA) can be used to derive the impact of different input variables on hydrological target variables. SA investigates the response of a modeled variable to the variation of model input variables (Saltelli et al., 2004). For a local

10   sensitivity analysis (LSA) the model inputs are varied around a point (often an 'optimum' point) in the model input space. Global sensitivity analysis (GSA) assesses the sensitivity of a model output for the entire feasible range of model inputs (Gupta and Razavi, 2017; Pianosi et al., 2016). Compared to LSA, GSA usually requires a larger number of computations. Thus, a substantial part of recent GSA literature focuses on the computational efficiency and the robustness of GSA methods (e.g. Pianosi and Wagener, 2015; Razavi and Gupta, 2016a; Sarrazin et al., 2016; Cuntz et al., 2015; Rakovec et al., 2014), but also

15   on increasing the insight into modeled systems from a certain number of model evaluations (e.g. Borgonovo et al., 2017; Dai et al., 2017; Guse et al., 2016a; Massmann et al., 2014; Razavi and Gupta, 2016a).

The complexity and computational demand of a model determine the feasible number of model evaluations and thereby the applicability of a SA method (Razavi and Gupta, 2015). Large atmospheric model applications, for instance, only allow a LSA with a few model evaluations (Gupta and Razavi, 2017; Pianosi et al., 2016). Environmental model applications are

20   usually less computationally expensive and allow a more extensive GSA, illustrated in many environmental modeling studies (e.g. Guse et al., 2016b; Haghnegahdar et al., 2017; Massmann and Holzmann, 2015; Razavi and Gupta, 2016b; Sarrazin et al., 2016). Most applications utilize GSA to identify influential model parameters and to rank model parameters according to their influence on model outputs. Model parameters are usually continuous model inputs. (Saltelli et al., 2008; Baroni and Tarantola, 2014).

25   Although it is possible to implement composite model inputs (e.g. climate scenarios that affect several climate variables at the same time, or land use scenarios that can impact the entire model setup) in a GSA and therefore to employ GSA in impact studies, a consideration of discrete and composite model inputs can constrain the applicability of GSA and complicate the implementation (Baroni and Tarantola, 2014). In impact studies, the response of an environmental variable to a (future) change in a model input is usually inferred by implementing a scenario realization of the respective model input in a model setup.

30   From an SA perspective, this approach is equivalent to a local 'one-at-a-time' (OAT) assessment of the model input sensitivity (Saltelli and Annoni, 2010; Baroni and Tarantola, 2014). A local OAT analysis however presumes linear models and non-correlated inputs which are hardly true for any environmental model application (Rosolem et al., 2012; Baroni and Tarantola, 2014). Thus, to account for interactions of model inputs and model non-linearities the application of GSA is recommended instead (Saltelli and Annoni, 2010; Saltelli and Tarantola, 2002; Baroni and Tarantola, 2014).

Yet, a few studies implemented discrete and composite model inputs in GSA. With the Generalized Probabilistic Framework, Baroni and Tarantola (2014) rendered a solid basis for the implementation of correlated, non-continuous model inputs in GSA and applied the variance-based SA method of Sobol (1993) to assess the response of soil moisture, evapotranspiration, and soil water fluxes to uncertainties in meteorological input data, crop parameters, soil properties, model structure, and observation data. In a synthetic example, Dai and Ye (2015) performed model and scenario averaging to assess the impact of different model structures and scenarios of precipitation on groundwater flow and reactive transport in the soil. In a more recent study, Dai et al. (2017) employed the method of Sobol to identify the relevant system processes for groundwater flow and reactive transport represented in different model structures. Savage et al. (2016) applied GSA to identify the dominant controls in the calculation of flood inundation, to assess whether a high spatial resolution of the flood inundation model or the model parametrization is dominating the simulation. The mentioned studies illustrate the use of GSA with discrete and composite model inputs. Anderson et al. (2014) and Butler et al. (2014) highlight the importance of assessing the uncertainty of future climate change impacts and the identification of relevant drivers and their interactions for climate policy making.

In this paper we demonstrate the utility of GSA and uncertainty analysis in a comprehensive setting of an environmental model impact study and address the following points:

- We apply GSA in two environmental modeling impact studies to identify the dominant sources of uncertainties for the simulation of discharge and nitrate-nitrogen (NO_3^--N) loads. We analyze the impacts of different spatial aggregations of the model setup and different model parametrizations and assess the effects of changes in the land use, point source emissions, and the future climate.

- We analyze the resulting uncertainties in the simulation of the long-term monthly mean discharge and monthly sums of NO_3^--N loads, as well as flow duration curves (FDCs) of daily discharge and daily NO_3^--N loads visually. We present ways to visualize the discrete model inputs that provide further insights into the relationships of uncertainties in the simulations and different properties of the discrete realizations of the model inputs.

- Based on the GSA and the visual analysis of the simulated uncertainties we are able to draw conclusion on the simulation of discharge and NO_3^--N loads as impacted by the model setup, model parametrization and the future scenarios of land use, point source emissions and climate. These conclusions are of course limited to assumptions made in the model setup and in the development of the scenarios.

The paper is structured in the following way: Section 2 contains an overview of the two investigated catchments, the Soil and Water Assessment Tool (SWAT, Arnold et al., 1998) that we implemented in this study, and the preparation of the model input data that we used in the model setup. In Section 2.4 we describe the setup of the SWAT model with different spatial aggregations and illustrate the pre-processing of the SWAT model setups that was necessary to identify the sensitive SWAT model parameters and to define non-unique parameter sets for all model setups. The scenarios of land use, point source emissions and the climate together with the input data and pre-processing to develop the individual scenarios are specified in Section 2.5. Section 2.6 combines the SWAT model setups, the defined non-unique model parametrizations and the developed scenarios of land use,

point source emissions and climate in the GSA and explains the methods we applied to analyze the sources of uncertainties for the simulation of discharge and NO_3^--N loads. The results of the combined GSA framework and the visual analysis are provided in Section 3. We discuss the findings of the GSA application and the visual analysis of the simulation uncertainties for the two case studies in Section 4 and address the specific assumptions that we made during the model setup and the development of the scenarios.

2   Materials and Methods

2.1   Study sites

The two investigated catchments (Schwechat and Raab) are representative examples for river systems for the eastern region of Austria. Both rivers have their origin in the forested foothills of the limestone Alps with a pre-alpine character and a low anthropogenic impact. The lower parts of both catchments are characterized by human activities, with primarily urban settlements and agricultural uses in the plains of the Schwechat catchment and dominant industrial activities and agricultural land uses in the valley bottom of the Raab catchment (Fig. 1 and Tables A3 and A4).

The Schwechat river has its source in the Vienna woods at the northeastern boundary of the Northern Limestone Alps with a maximum altitude of 893 m a.s.l. After a natural flow section in the narrow and dominantly forested valley of the "Helenental" (70% of the total catchment area. See Table A3), the Schwechat drains into the Vienna basin with flat topography and a predominance of agriculture, viniculture and settlement areas. The main agricultural crops are winter wheat and summer wheat. Larger areas in the upper part of the catchment are used as pastures (~10% of the total area). The largest settlement is the city of Baden with a population of approximately 26000 inhabitants, while smaller settlements are scattered over the catchment. All municipal wastewaters are collected in three wastewater treatment plants (WWTP, black triangles in Fig. 1), where the the WWTP Baden is the most relevant one with a capacity of 45000 population equivalents (PE). All WWTPs perform carbon removal, nitrification, denitrification and enhanced phosphorus removal. Due to the close proximity to the city of Vienna population growth is a likely prospect for the settlement areas in the lower part of the catchment. The part of the catchment considered in this study has its outlet next to the city of Traiskirchen at an altitude of 185 m a.s.l. and covers an area of approximately 275 km². The long term mean annual precipitation in the Vienna Basin is around 620 mm/yr and the mean annual temperature is 9.9°C.

The Raab river originates at the edge of the southeastern Alps. These are characterized by low mountain ranges with a maximum altitude of 1547 m a.s.l., mostly covered by forests (~42% of the total catchment area. See Table A4). The Raab flows through the southern part of Austria and crosses the boarder to Hungary close to the city of Neumarkt an der Raab at an altitude of 232 m a.s.l. The case study encompasses the Austrian part of the Raab with a catchment area of approximately 998 km². The long-stretched river valley is dominated by agricultural activities (~25 % of the total area), with urban areas in between. The slopes along the Raab are covered with heterogeneous patterns of forests, pasture areas and agricultural land use. The main agricultural crops are corn and oil seed pumpkins, but also wheat and vegetable production are common. While the urban areas are of similar small structure as in the Schwechat catchment, leather industries are present in the catchment
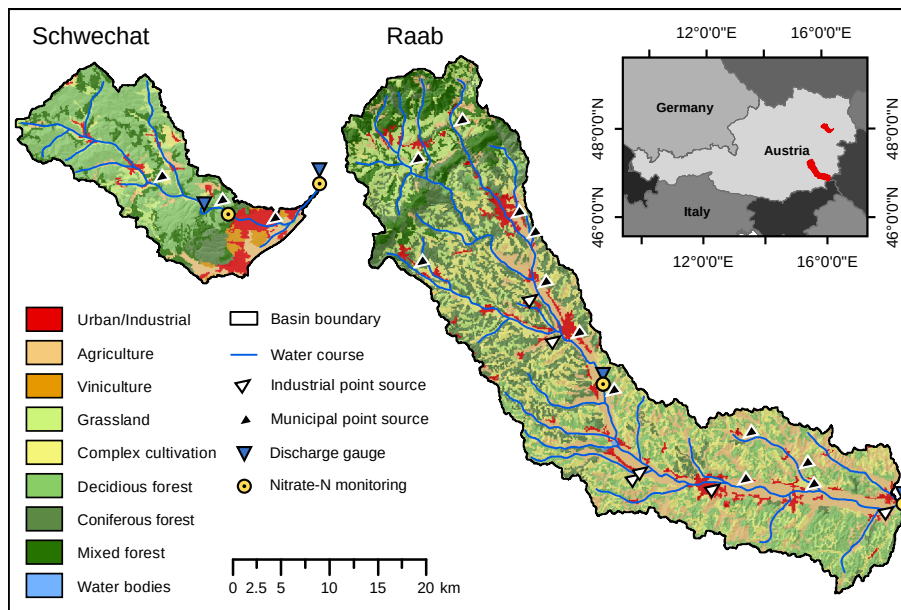
Figure 1. Study sites Schwechat (left) and Raab (right).

that release substantial nutrient inputs into the receiving waters, which has resulted in trans-boundary conflicts (Ruzicka et al., 2009). Municipal wastewaters in the Raab catchment are collected in 12 relevant WWTPs (black triangles in Fig. 1) that all have the same standards for wastewater treatment as in the Schwechat catchment, but have almost three times the total capacity (approximately 150000 PE). Six relevant industrial emitters are located along the main reach of the Raab river (white
5   triangles in Fig. 1) that all perform internal waste water treatment following the respective industry-specific regulations for wastewater treatment (e.g., BGBl. II Nr. 10/1999, 1999; BGBl. II Nr. 12/1999, 1999). The average annual precipitation in the Raab catchment is approximately 800 mm/yr and the long term annual mean temperature is 9.0°C.

2.2   The Soil and Water Assessment Tool (SWAT)

The SWAT model (Arnold et al., 1998) is a continuous, process based, semi-distributed eco-hydrological model. In this study
10   we implemented SWAT2012 (Rev.622) to simulate daily time series of discharge and NO_3^--N loads at the catchment outlets. The models' spatial reference to a catchment is given by a subdivision of the basin into subbasins. Areas containing the same land use, soil type and lying in the same slope range are lumped together in each subbasin to form hydrologic response units (HRUs). All processes on the land phase of each subbasin are calculated at the HRU scale and are further propagated into the water phase of each subbasin. The processes calculated on the land phase include water balance components such
15   as interception, infiltration, shallow and deep percolation, surface runoff, lateral flow, groundwater flow, plant uptake and evapotranspiration, or the pathways of nutrients such as the input through atmospheric deposition, or fertilizer application, the transformation into other forms of a nutrient and the transport through surface runoff, percolation, lateral flow and return flow

in the groundwater (Neitsch et al., 2011). In the water phase, the nutrients budgets are calculated. Following the calculation of the water balance and the nutrient budgets, the discharge, the nutrient loads and other substances are routed through the linked subbasins to the defined catchment outlet (Neitsch et al., 2011). The required input data to set up a model with SWAT are a digital elevation model (DEM), a raster land use map including the model parametrization and the performed management operations for each land use, a raster soil map with soil physical and chemical parameters for all soil layers, and meteorological input data.

2.3   Model input data and data preparation

A DEM with a 10 m resolution was available for Austria from an airborne laser scan (Geoland.at, 2015). Based on the DEM we defined three slope classes with slopes of 0-3%, 3-8%, and >8% in the HRU definition step.

CORINE land cover (EEA, 2015) served as the base land use map to which more detailed agricultural data was added. CORINE does not classify agricultural land uses into crop types. Therefore, tabular data of agricultural land uses at the municipal level derived from the 2010 Austrian agronomic census (Statistik Austria, 2015b) was superimposed onto CORINE data by randomly distributing crops according to the crops' areal share at the municipal level to CORINE pixels containing agricultural and complex cultivation land use. Typical time windows for planting, fertilizer application, tillage and harvest were derived from field experiment records for the individual crops (Land NÖ, 2015) and written to the HRU management files. The management dates were randomized for all HRUs within the time windows derived for a management operation. Dates with strong rainfall or a high soil moisture potential were not used for scheduling management operations. With 70.0% and 42.3% forest land uses where the most dominant land uses in the Schwechat and the Raab catchments, respectively. The SWAT model setups differentiated between deciduous forests, coniferous forests and mixed forests, derived from CORINE land cover (see Tables A3 and A4). All HRUs with one of the three forest types as land use were parameterized with an initial biomass and an initial leave area index to simulate intact forests in both catchments.

The SoilGrids data base (Hengl et al., 2017) is a consistent global soil information system that provides soil physical and chemical parameters at a 250m grid resolution and seven soil depths. We utilized the available soil parameters from SoilGrids and estimated further required soil parameters with pedo-transferfunctions provided by the R package euptf (Tóth et al., 2015). The seven available soil depths from the SoilGrids data were aggregated to three soil depths (0-30cm, 30-100cm, and 100-200cm), and the gridded data were clustered into soil classes applying kmeans clustering (R Core Team, 2017, Hartigan and Wong (1979)) resulting in 14 and 8 "optimum" soil classes for the rivers Schwechat and Raab respectively.

Meteorological input data was available from the INCA system developed and operated by the Central Institute for Meteorology and Geodynamics of Austria (ZAMG; Haiden et al., 2011). INCA provides reanalysis data of precipitation and temperature on 1km grid resolution for Austria with a temporal resolution of 15 minutes for precipitation and 60 minutes for temperature in the period from 2003 to 2015. For all SWAT model setups, daily precipitation sums and daily minimum and maximum temperatures were temporally and spatially aggregated for the model subbasins.

Point source emission data was available from external emission monitoring of municipal WWTP greater than 2000 PE according to BGBl. 1996/210 (1996) for both catchments. Municipal WWTP larger than 2000 PE are responsible for 99.2%

Table 1. Input data for the SWAT model setup, the data sources, and data processing steps.

Input data set	Data source	Data preparation
Topography	DEM Austria (Geoland.at, 2015)	Digital Elevation Model for Austria in 10m resolution.
Land use	CORINE Landcover (EEA, 2015), 2010 Austrian agronomic census (Statistik Austria, 2015b)	Basis: CORINE Land cover, Agricultural areas re-sampled with statistical information from 2010 Austrian agronomic census.
Soil data	soilgrids.org (Hengl et al., 2017), euptf (Tóth et al., 2015)	Basis: SoilGrids 250m resolution in 7 depths. Clustered in space and and aggregated over depth. Further SWAT soil parameters derived using pedotransfer functions.
Meteorology	INCA (Haiden et al., 2011)	Precipitation and temperature data in 1km resolution.
Agricultural practices	Statistik Austria (2015b), Land NÖ (2015)	Derive time periods and sequences of field management practices from field experiments.
Point source emissions	External monitoring, Internal records of WWTPs	Time series and point measurements of discharge and NO_3^--N concentrations.

and 86.3% of municipal point source emissions in the Schwechat and the Raab catchments respectively. Thus, these data cover a substantial part of the municipal emissions. Additionally, daily and weekly internal monitoring data was available for some large WWTP schemes. In most cases however, only information on NO_3^--N emissions was provided. A general budgeting of nitrogen emissions however showed, that the substantial share of total nitrogen is emitted in form of NO_3^--N(87% in the Schwechat catchment and 89% in the Raab catchment). For industrial emitters monthly and annual records from internal and external monitoring agencies were available and only allowed an estimation of industrial emissions with coarse temporal resolution, while covering the annual budgets. Again, mainly data for NO_3^--N emissions were available. Although, nitrogen is emitted in different forms the available data basis only allowed to consider NO_3^--N loads contributed by point sources.

Table 1 provides an overview of the model input data that was used for the SWAT model setup.

Hourly observations of discharge were available for the period from 2003 to 2015 at two gauges for the Schwechat and the Raab each (Fig. 1). NO_3^--N concentration readings with varying time intervals of 5 to 15 minutes were available at two stations in both catchments (yellow circles in Fig. 1) for selected time periods resulting from monitoring campaigns at the rivers Schwechat (BMLFUW, 2013) and Raab (BMLFUW, 2015a, b). SWAT simulates output variables with daily time steps. To compare the observations with the modeled SWAT outputs of discharge and NO_3^--N loads, daily NO_3^--N loads and daily mean discharge were calculated from the observation data.

Table 2. SWAT model setups for the Schwechat and the Raab catchment including the numbers of subbasins and the number of HRUs for each setup.

	Schwechat			Raab	
Setup	# Subbasin	# HRU	Setup	# Subbasin	# HRU
sw_14_full	14	1434	rb_54_full	54	5349
sw_14_thru	14	196	rb_54_thru	54	954
sw_03_full	3	606	rb_30_full	30	3516
sw_03_thru	3	64	rb_30_thru	30	584
			rb_04_full	4	755
			rb_04_thru	4	115

2.4 Model setup, parameter selection and identification of non-unique parameter sets

Graphical GIS user interfaces such as ArcSWAT (Winchell et al., 2015) or QSWAT (Dile et al., 2016) facilitate the setup of SWAT models. Yet, a model setup requires the modeler to define the number of subbasins as well as the number of HRUs (e.g. by removing HRUs with areas below a certain threshold from the setup and apportion their areas to the remaining HRUs). The size and the number of subbasins in a model setup can affect the process simulations and the resulting model outputs (Jha et al., 2004; Momm et al., 2017; Tripathi et al., 2006). Removing small HRUs from the model setup and allocating their areas to the remaining HRUs affects the distribution of land use, soil types, and slope classes and thus can impact the model simulations substantially (Jha et al., 2004).

We used the ArcSWAT plugin (Version2012.10_1.14) together with ArcGIS 10.1 (ESRI, 2012) for the model setup. For both case studies we set up the SWAT model with different numbers of subbasins, whereby we prepared model setups with the full number of HRUs and respective setups with a reduced number of HRUs for each catchment.

In total, we set up four SWAT models, two with 3 and two with 14 subbasins for the Schwechat catchment and six models for the Raab catchments with two each of 4, 29, and 54 subbasins. For the full HRU setups we kept the resulting HRUs unmodified. For the model setups with a reduced number of HRUs we eliminated small HRUs. We determined thresholds for land use, soil, and slope classes to remove HRUs that have an area below these found thresholds. The thresholds were determined using the R package 'topHRU' (Strauch et al., 2016). 'topHRU' enables to find thresholds that minimize the number of HRUs of a SWAT model setup while minimizing the aggregation error (sum of changes in the areas of land uses, soils and slope classes of the reduced set of HRUs compared to the full HRU setup). To maintain a comparability between the reduced HRU setups thresholds were selected that result in an aggregation error of 5% in all reduced HRU model setups. Table 2 gives an overview of the final model setups for both case studies.

In a parameter screening, we applied a GSA to the simulations of discharge and NO_3^--N loads at the catchment outlets of all SWAT model setups to identify influential model parameters. Initially, 42 model parameters were selected that are frequently calibrated in SWAT model setups to simulate discharge and NO_3^--N loads. The SWAT model setup initializes the

model parameters using values obtained from the SWAT data bases (either standard values or user defined, e.g. by pedotransfer functions). The selected initial ranges to modify the model parameters and the selected types of parameter changes (e.g. replace parameter values globally or modify a spatially distributed parameter field by a fraction of a parameter) reflect typical procedures often found in SWAT model calibration studies. An overview of the model parameters that were identified as influential and that were further used in the model impact study is provided in Table A1.

We employed the STAR VARS approach (Razavi and Gupta, 2016a, b) to screen and rank the model parameters. STAR VARS utilizes variograms along each model input dimension of the input space to infer each model inputs influence on a target variable over different scales (where short lag distances approximate the derivative based method of Morris (Morris, 1991) and long distances the method of Sobol (Sobol, 1993)). The calculation of the variograms is based on the tailored STAR sampling design where "star center" points are randomly sampled in the input space. For each center point cross sections are sampled along the input factor dimensions with an equally spaced interval. For each sampled input combination the model is evaluated and variograms along the response surface are calculated. Razavi and Gupta (2016a) proposed integrated measures of the variograms as measures of sensitivity, where the measures $IVARS_{10}$, $IVARS_{30}$, and $IVARS_{50}$ represent the integrals over 10%, 30%, and 50% of each input dimension respectively and therefore provide the sensitivity of a target variable to a model input over different scales. A detailed description of the method is provided in Razavi and Gupta (2016a) and the STAR sampling is outlined in Razavi and Gupta (2016b). The method proved to be robust and computationally efficient for high dimensional problems (e.g., Razavi and Gupta, 2016b; Haghnegahdar et al., 2017; Sheikholeslami et al., 2019; Haghnegahdar and Razavi, 2017).

We drew STAR samples (Razavi and Gupta, 2016b) with 50 center points and ten parameter samples per parameter dimension that resulted in 18950 parameter combinations per model setup. To calculate the target variables we used the Nash Sutcliffe Efficiency criterion (NSE, Nash and Sutcliffe, 1970), the Kling Gupta Efficiency criterion (KGE), including its three components (Gupta et al., 2009), and a refined version of the Index of Agreement (Willmott et al., 2012) to evaluate the simulated time series of daily mean discharge and daily sums NO_3^--N loads. Additionally, we applied the ratio of the root mean square error and standard deviation (RSR, (Moriasi et al., 2007)) to evaluate different segments of the FDCs of daily discharge and daily NO_3^--N load simulations (Pfannerstill et al., 2014; Haas et al., 2016). A model parameter was considered to be sensitive if it showed a relative sensitivity of 10% compared to the most sensitive parameter with respect to a specific objective criterion for at least one of the employed objective criteria.

The performed GSA for the model parameters of the different model setups of the Schwechat catchment and the Raab catchment respectively showed very similar results independent of the number of subbasins and HRUs of the individual model setups (Fig. A1). Therefore, for the impact study the same set of model parameters was considered as influential for all model setups of the Schwechat and the Raab, respectively. In total, 19 parameters for the Schwechat and 16 parameters for the Raab were identified to be influential for the analyzed target variables (Table A1).

To represent the model parametrization as an input in the subsequent sensitivity and uncertainty analysis of the environmental impact study, non-unique parameter sets were identified for the Schwechat and the Raab catchments, respectively. The preceding parameter SA revealed that changes in the model parameter values influenced the simulations similarly independent

of the subbasin and HRU configurations in the Schwechat and the Raab catchment, respectively. As a consequence, but also to facilitate the separation of the effects of the model setup and the model parametrization in the analysis, we selected parameter combinations as non-unique ones that result in simulations of daily discharge and NO_3^--N loads that fulfill certain objective criteria together with all model setups of the Schwechat and the Raab, respectively. For the respective 19 and 16 influential

5   model parameters we randomly sampled 100000 parameter combinations and simulated daily discharge and NO_3^--N loads with all model setups of the Schwechat and the Raab catchments. We evaluated the simulations with the following criteria to accept a parameter set: KGE > 0.5 for daily discharge at the catchment outlets, KGE > 0.4 for daily NO_3^--N loads at the gauges with longer continuous records (in both case studies the gauging point within the catchment and not at the catchment outlet), percentage bias (Gupta et al., 1999) < 50% for NO_3^--N loads, and absolute RSR < 1 for different discharge and NO_3^--N load

10   (according to Pfannerstill et al., 2014; Haas et al., 2016). In total, we identified 43 and 52 behavioral parameter combinations for the Schwechat and the Raab catchments, respectively. The ability of the selected parameter sets used with the different model setups to reproduce the observed data is illustrated in Fig. A2. The initial and final ranges of parameter changes are shown in Table A2. The 43 and 52 parameter combinations are additionally illustrated in parallel coordinate plots for the Schwechat and the Raab in Fig. A3 to show any clustering of individual parameters and interactions between parameters.

15   **2.5   Scenario definition**

The study involves future changes of the land use, point source emissions, and the climate. The uncertainties of these variables are expressed as discrete scenarios.

For the land use change scenarios, two scenario story lines (Rounsevell and Metzger, 2010) were developed for the Schwechat and the Raab catchments. A "business-as-usual" scenario extrapolates the observable trends in land use change to the future

20   (2071 to 2100), while a second "extensive" scenario assumes an extensification of agricultural activities and other intensive land uses in both catchments (Table A5).

In the Schwechat catchment population growth is the strongest factor for a future change in land use (Statistik Austria, 2015a, 2016). Hence, a transformation from extensive pasture land (-35%) to urban land use and an increase of dense urban areas describe the "business-as-usual" scenario. The "extensive" scenario assumes no change in population and a shift of half

25   of the wheat producing area to extensive pastures.

Since 1970, the areas for corn production increased by 220% in the Raab catchment, mostly for biogas production and at the expense of sugar beets and cereals (Statistik Austria, 2017). For the "business-as-usual" scenario, an increase in the corn area by a further 100% until the end of the century was assumed, replacing extensive pastures (-75%), sugar beets (-80%), legumes (-70%), and winter wheat (-30%).

30   Groundwater protection measures lead to strict regulations for fertilizer application in the Leibnitzerfeld region adjacent to the Raab catchment (LGBl. Nr. 39/2015, 2015). Therefore, the "extensive" scenario assumes an adoption of similar nitrogen regulations in the Raab catchment. Thus, decreasing areas with intensive fertilizer application, such as corn by 50% and transforming these areas to extensive pasture land was carried out in this scenario.

Two municipal point source emission scenarios for both case studies (Table A6) and two industrial point source emission scenarios for the Raab catchment (Table A7) were developed. The future change in municipal emissions was assumed to be directly related to the change in population. For all provinces in the Schwechat basin future scenarios predict an average population growth of 32% (Statistik Austria, 2015a, 2016). The predictions of the population development in the provinces of the Raab are contradicting, with predicted changes between +2.3% (Statistik Austria, 2015a) and -20.4% (Amt d. Stmk LReg, 2016).

In the Raab catchment 94% of the industrial point source emissions stem from the leather industry and almost 70% of the industrial point source emissions are caused by one leather manufacturing company. Thus, industrial emission scenarios were developed for that particular manufacturer. As boundaries for the production, we defined an upper environmental boundary and a lower economical boundary for the prediction of future industrial emissions. Based on an assessment of effluent dilution (ÖWAV, 2010), current environmental regulations (BGBl. II 2010/99, 2010; and BGBl. II 2006/96, 2006) allow an increase of 30% in emissions from that leather producer, resulting in a total increase in industrial emissions of 22.6%. Assuming a relocation of the two manufacturing sites of that leather producer to outside of the catchment would stop their emissions into the Raab, reducing the total industrial point emissions by 75.2%.

Future climate change was considered with 22 downscaled and bias corrected climate change scenarios (Table A8). Regional climate simulations were obtained from the EU-CORDEX project (Jacob et al., 2014), providing 11 GCM-RCM simulations for the emission scenarios RCP4.5 (Smith and Wigley, 2006; Wise et al., 2009) and RCP8.5 (Riahi et al., 2007) respectively. In this study we utilized daily precipitation sums and daily minimum and maximum temperatures for the time period 2071 to 2100. The EURO-CORDEX climate simulations are available at a spatial resolution of 12.5 km (EUR-11) (Jacob et al., 2014). Statistical downscaling (Zorita and Von Storch, 1999) was applied to prepare all climate simulations at a resolution of 1 km. To correct downscaling errors (e.g. Haslinger et al., 2013; Muerth et al., 2013), bias correction (Teutschbein and Seibert, 2013) was applied to the climate simulations employing quantile mapping (Hempel et al., 2013). Downscaling and bias correction were performed for the historical period 1971 to 2000, involving the reanalysis datasets SPARTACUS (Hiebl and Frei, 2016) for minimum, mean and maximum temperature and GPARD (Hofstätter et al., 2013) for daily precipitation sums.

2.6 Analysis

Table 3 summarizes the land use change, point source emissions, and climate change and the model setups and model parametrizations that were used for the analysis of simulated discharge and NO_3^--N loads in the Schwechat and the Raab catchments. In total, 7000 combinations of land use, point source emissions, climate, model setups and model parametrizations were drawn for both case studies applying a quasi random sampling. The number of combinations results from previous experiments that applying the SA method of Sobol (results not shown) using the sampling strategy proposed by Saltelli and Tarantola (2002) with a base sample size $N_b = 1000$ and a total sample size of $N = N_b(k+2)$, where k is the number of model inputs that are analyzed. All sampled combinations were assembled to executable SWAT models. Daily discharge and daily NO_3^--N loads at the outlets of the Schwechat and the Raab catchments were simulated for the period from 2071 to 2100.

Table 3. SWAT inputs implemented in the sensitivity analysis case studies and their numbers of discrete realizations for the Schwechat and the Raab catchments.

Input	# Values		Details on values
	Schwechat	Raab	
Land use scenario	2	2	one "extensive", one "business-as-usual"
Point source scenario	2	4	Population growth: optimistic/pessimistic , Industry Raab: production increase/resettlement
Climate scenario	22	22	11 RCP4.5, 11 RCP8.5, period: 2071-2100
Model setup	4	6	Raab: 54, 30, 4 subbasins with/without HRU reduction, Schwechat: 14, 3 subbasins with/without HRU reduction
Parametrization	43	52	KGE discharge >0.5, KGE NO_3^--N >0.4, pbias NO_3^--N <50%

The analysis of discharge and NO_3^--N loads follows two main goals i) to identify the dominant controls on the simulation of discharge and NO_3^--N loads in the two case studies and ii) to assess how the considered inputs control the simulation of discharge and NO_3^--N loads.

2.6.1 Global sensitivity analysis

5 To measure the relative importance of the developed model input scenarios, the model setup and the parametrization on the simulation of daily discharge and daily NO_3^--N loads, we employed GSA using the PAWN sensitivity index (Pianosi and Wagener, 2015). PAWN employs the empirical cumulative distribution function (CDF) of a target variable to infer the model input influence (Pianosi and Wagener, 2015). PAWN is moment-independent and was found to be a robust measure for sensitivity of non-symmetrically distributed outputs of environmental models (Pianosi and Wagener, 2015; Zadeh et al., 2017).

10 PAWN expresses the sensitivity of a target variable x to a model input x by computing a distance measure between the unconditional CDF $F_y(y)$ (where all model inputs are perturbed) and the conditional CDF $F_{(y|x_i)}(y)$ (where the model input of interest is fixed and all others are perturbed). Pianosi and Wagener (2015) proposed is the Kolmogorov-Smirnov test statistics as a distance measure. The distance $KS_j(x_i^j)$ between the CDFs for the model input x_i fixed at a value $x_i = x_i^j$ is defined as:

$$KS_j(x_i^j) = \left\| F_y(y) - F_{y|x_i, x_i = x_i^j}(y) \right\|_y \tag{1}$$

15 To assess the overall sensitivity considering all fixed values of x_i, the values of $KS_j(x_i^j)$ are summarized for all j sampling points. A summary statistics (Pianosi and Wagener (2015) suggested e.g. median or maximum) is applied to compute the PAWN index T_i for the model input x_i. The model inputs that are analyzed in this study strongly differ in their numbers of discrete realizations. Further, the distribution of the resulting Kolmogorov Smirnov distances can be highly skewed (e.g. the majority of discrete realizations has a low impact, while a few realizations strongly influence the simulation). Therefore, the

20 significance of an average sensitivity of a target variable y_i to a model input x_i is questionable. In a setting where the strongest

impact of a model input x_i on a target variable y_i is of major interest the application of a maximum statistics is beneficial. Hence, the PAWN sensitivity index is defined here as:

$$T_i = \max_{x_i = x_i^1 \ldots x_i^{n_i}} \left(KS_j(x_i^j) \right) \tag{2}$$

The values $x_i = x_i^1, \ldots, x_i^j, \ldots, x_i^{n_i}$ are the n_i discrete realizations of the input x_i. The resulting PAWN sensitivity index
5   varies between 0 and 1 where a lower value of T_i implies a lower influence of the input x_i on the target variable y.

Pianosi and Wagener (2015) introduced the PAWN sensitivity method using a specifically tailored sampling design to infer the PAWN indices T_i for continuous model inputs x_i. The proposed sampling scheme suggests to draw N_c conditional samples at n randomly sampled points of each influencing variable x_i, where x_i is fixed at a value $x_i = x_i^j$ while all others are perturbed. Recently, Pianosi and Wagener (2018) extended the applicability of the PAWN sensitivity method to estimate T_i from a generic
10   random sample of continuous model inputs. To approximate T_i the generic sample N is split into n segments along each model input dimension resulting in conditional samples N_c with an approximate size of N/n. We employed the proposed updated sampling strategy and adapted it for the use with discrete model inputs. A sample of the size N was drawn. For each model input combination every model input was sampled randomly from its discrete realizations. To infer $KS_j(x_i)$ for all discrete values x_i^j of a model input x_i the sample N was split into subsets for all n_i discrete values, resulting in subsets of the size
15   N/n_i on average. It is important to consider, that the subset size depends on the number of discrete values n_i of a model input x_i, while the subsets resulting from the sampling scheme proposed by Pianosi and Wagener (2018) had an average size of N/n for all model inputs x_i.

To account for the effect of different numbers of discrete realizations of the analyzed inputs, but also to assess whether the number of drawn samples of input combinations ($N = 7000$) was sufficient to perform a GSA with PAWN, confidence intervals
20   were calculated for the PAWN indices applying bootstrapping (Hinkley, 1988; Efron, 1987) using the R package 'boot' (Canty and Ripley, 2017). To calculate the bootstrap mean and the 95% confidence intervals, 1000 bootstrap replicates were drawn (as demonstrated in Sarrazin et al. (2016)).

Signature measures of discharge and NO_3^--N loads were used as target variables y. Signature measures are measures that describe specific characteristics of simulated time series (Euser et al., 2013) (in this case of daily mean discharge and daily sums
25   of NO_3^--N loads). We calculated quantile values (0.01, 0.05, 0.20, 0.70, 0.95, and 0.99) of daily discharge and daily NO_3^--N loads, long-term mean discharges and long-term mean sums of NO_3^--N loads on an annual basis and for the meteorological seasons spring, summer, autumn, and winter, and mean NO_3^--N concentrations for different ranges of discharge quantiles (very high discharge (above 0.95 quantile), high discharge (0.95 to 0.70 quantile), medium discharge (0.70 to 0.20 quantile), low discharge (0.20 to 0.05 quantile), and very low discharge (below 0.05 quantile)).

30   **2.6.2   Visual analysis of the simulation uncertainties**

To investigate how the inputs of land use change, changes in point source emissions, climate change, the model setup or the model parametrization control the simulation of discharge and NO_3^--N loads, we analyzed the simulation outputs and their as-

sociated uncertainties visually. The 7000 assembled combinations of model inputs, model setups and parametrizations resulted in ranges of simulated discharge and NO_3^--N loads. All executed model setups represent plausible realizations of the future conditions in both catchments to simulate future discharge and NO_3^--N loads. Thus, the overall simulation uncertainties of simulated discharge and NO_3^--N loads comprise all 7000 simulations of the Schwechat and the Raab catchments, respectively.

5   We visually analyzed the uncertainty bands (no thresholds were set) of the simulations of the long-term mean monthly specific discharge, the long-term mean monthly sums of NO_3^--N loads and the FDCs of daily discharge and daily NO_3^--N loads. These variables are related to a wide range of the signature measures that were analyzed in the GSA and thus allow a comparison of the GSA results with the results of the visual uncertainty analysis.

    The low number of possible values taken by each input allowed a more detailed analysis of their effect on the simulated 10 uncertainties, by subsetting the uncertainty bands of the discharge and NO_3^--N load simulations with respect to the individual realizations of the analyzed model input. The separated simulation uncertainty bands were additionally colored with respect to the specific properties of an input, such as the temperature or precipitation anomalies of each climate scenario compared to historical records. These color ranges greatly facilitated identifying the dominant controls of the simulation.

3   Results

15 ### 3.1   Sensitivity analysis

Fig. 2 summarizes the influence of the implemented land use, point source emission, climate scenarios, the different model setups and the model parametrizations for the simulation of future discharge and NO_3^--N loads in the Schwechat (left) and the Raab (right) catchments. Each plot panel shows the calculated PAWN indices for the analyzed target variables for one model input in a catchment. Related target variables are grouped by colors to support the interpretability (e.g. to identify changes in 20 sensitivity from high to low discharge). In its entity each panel provides a general overview of the importance of an input for the simulation of discharge and NO_3^--N loads. Individual PAWN indices (a single bar in a plot panel) highlight the importance of an input for the simulation of specific characteristics of the time series of discharge and NO_3^--N loads.

    The white boxes on top of each bar show the bootstrap means and the 95% confidence intervals (CI) of each PAWN index and therefore provides an indicator for the adequacy of the sample size that was used to perform the analysis and the impact of 25 differing numbers of discrete values of the analyzed input variables. In general the bootstrapping resulted in narrow confidence intervals (maximum +0.05 and -0.08) for all analyzed model inputs and all signature measures providing high confidence in the resulting sensitivities. Although the numbers of discrete realizations of the analyzed model inputs (e.g. only 2 land use scenarios, but 43 and 52 model parametrizations) differ strongly and therefore result in different subset sizes to calculate the PAWN indices, no substantial differences in the confidence intervals is visible.

30   The land use scenarios applied to SWAT demonstrated a rather negligible impact on all signature measures, with mean PAWN indices below 0.05 and 0.07 and confidence intervals in the same range for the Schwechat and Raab respectively (first row Fig. 2). The point source scenarios, in contrast, showed a considerable influence on the signature measures of NO_3^--N loads and concentrations in the Raab case study, while the impacts of the point sources in the Schwechat case study were

negligibly low (second row Fig. 2). Thus, based on the implemented point source emission scenarios, industrial emitters in the Raab catchment are relevant for the development of in-stream NO_3^--N loads and concentrations, particularly for low discharges and low NO_3^--N loads. The importance of the industrial point sources in SWAT increases when higher NO_3^--N load quantiles (low NO_3^--N loads, from dark yellow to light yellow in Fig. 2)) and NO_3^--N concentrations for low discharges (from dark red to light red in Fig. 2) are simulated, which is evident from an increase in the mean PAWN index from 0.11 to 0.49 and 0.22 to 0.43, respectively. The climate scenarios and the model parametrizations show respective decreases in their importance for the simulation of low NO_3^--N loads and NO_3^--N concentrations for low discharges (with decreases in the mean PAWN index from 0.71 to 0.28 for the climate scenarios' influence on NO_3^--N loads and from 0.79 to 0.36 for model parametrization's influence on NO_3^--N concentrations).

The implemented climate scenarios showed large impacts on all calculated signature measures of discharge and NO_3^--N loads (third row Fig. 2). The mean PAWN indices range between 0.25 to 0.90 and 0.25 to 0.96 for the Schwechat and the Raab, respectively. The climate scenarios were the most relevant inputs for the simulation of seasonal mean discharges and seasonal sums of NO_3^--N loads. For the simulation of low discharge quantiles (large daily discharges) climate scenarios showed the highest relevance. For the simulation of low discharges however, the importance of the climate scenarios decreases, while the model parametrization becomes more relevant (from dark green to light green in Fig. 2). The mean PAWN indices of climate scenarios drop from 0.74 to 0.47 in the Schwechat catchment and from 0.82 to 0.51 for the simulation of lower discharges, while the mean PAWN indices for the model parametrization show respective increases from 0.43 to 0.87 and 0.44 to 0.80.

In general, the model parametrization was highly influential for all calculated signature measures and is comparable to that of the climate scenarios, with mean PAWN indices ranging between 0.43 to 0.90 in the Schwechat and 0.36 to 0.80 in the Raab (fifth row Fig. 2). Particularly, for the simulation of NO_3^--N concentrations the model parametrization was the most dominant control of the variable simulated. In contrast to the large impact of the model parametrization, the relevance of the model setup was much lower for the simulation of discharge and NO_3^--N loads and concentrations. Overall, values of the PAWN index for the choice of the model setup did not exceed 0.37, and were much smaller (two to five times) compared to the model parametrization. The model setups yielded insignificantly low PAWN indices for the majority of signature measures with values below 0.1 in the Raab case study (2.5 % CI almost 0 for many signature measures), indicating that the model setup had a low influence on most of the analyzed processes. Only for high discharges and large NO_3^--N loads a mean value for the PAWN index above 0.1 is visible.

3.2 Analysis of the simulation uncertainties of discharge and NO_3^--N loads

Using all 7000 combinations of land use, point source emissions, climate, model setups, and model parametrizations, the simulated discharges and NO_3^--N loads deviated by up to 350% (grey bands in Fig. 3) from the simulations of discharge and NO_3^--N loads in the reference period 2003 to 2015 (dashed line in Fig. 3). In the Schwechat (left column in Fig. 3) wider uncertainty bands are visible for the spring and early summer months. The results for the Raab catchment (right column) show wider uncertainty bands emerged for summer as well as for winter/early spring. A notable difference between the two case studies is how the simulations of long term monthly discharges and NO_3^--N loads in the reference period compare to the ranges
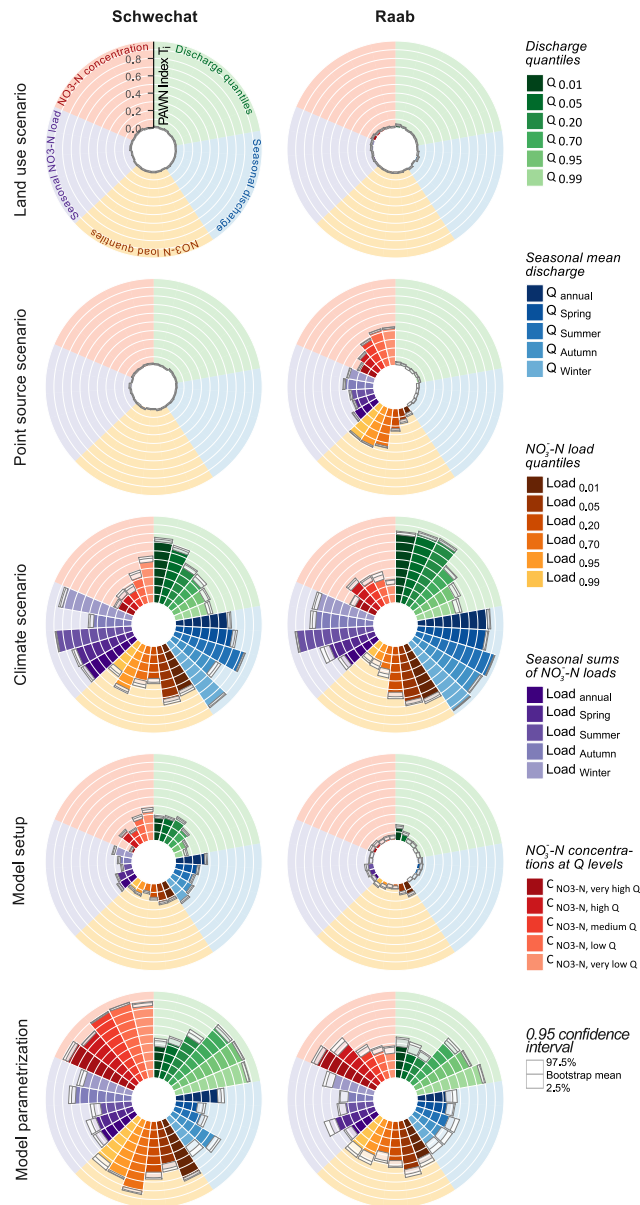
Figure 2. Sensitivities of signature measures of discharge and $NO_3^- - N$ loads in the Schwechat (left) and the Raab (right) catchment to the model inputs land use scenarios, point source scenarios, climate scenarios, the model setup, and the model parametrization. Each circle plot shows the set of PAWN indices calculated for the respective case study and model inputs. PAWN indices are illustrated in colored groups and clockwise order for discharge quantiles (green), seasonal long-term mean discharges (blue), quantiles of $NO_3^- - N$ loads (yellow), seasonal sums of $NO_3^- - N$ loads (purple), and mean $NO_3^- - N$ concentrations for discharge quantiles (red). The white boxes represent the bootstrap mean and the 95% confidence intervals for the calculated PAWN indices.
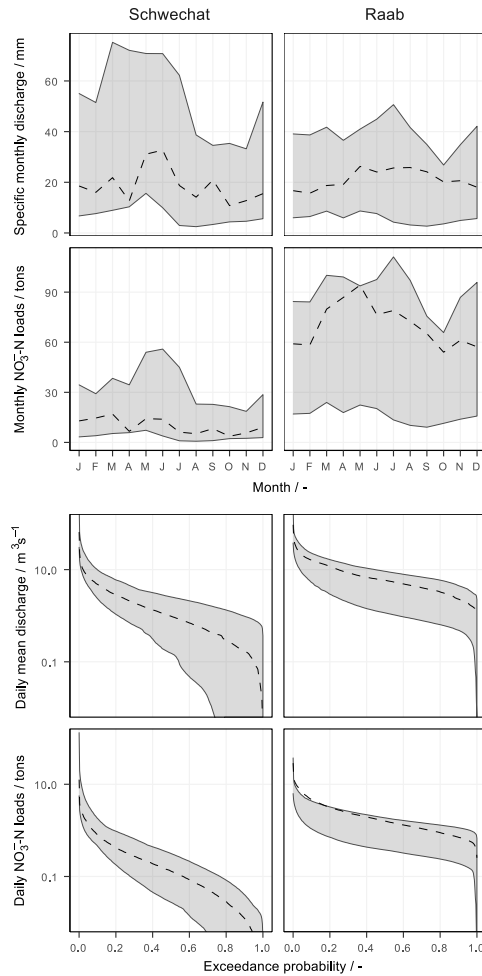
Figure 3. Simulated uncertainties resulting from the 7000 combinations of realizations of the influencing variables for the Schwechat (left) and the Raab (right). The grey bands illustrate the absolute ranges of simulated long-term mean monthly specific discharge (first row), long-term monthly sums of $NO_3^- - N$ loads (second row), FDCs of mean daily discharges (third row), and FDCs for daily sums of $NO_3^- - N$ loads (fourth row). The dashed lines show the best simulation of the historical reference period.

of future simulations. While the majority of model combinations for the Schwechat simulated larger discharges and NO_3^--N loads for all months in the future, for the Raab catchment the simulations of discharge and especially NO_3^--N loads are lower in comparison to the reference period.

The analyses of the uncertainty bands with respect to the implemented land use scenarios and the point source scenarios

5 fully confirm the results from the SA (Fig. 4). The attributed uncertainty bands for the two land use scenarios almost entirely overlap and show only minor deviations. A similar result is illustrated for the two point source scenarios in the Schwechat case study. The scenarios in the Raab catchment involved industrial point source emissions. The grouped uncertainty bands that

include scenarios with an increase in industrial production (red) and the uncertainty bands that include a decrease in industrial production (blue) show similar patterns. Yet, the blue and red uncertainty bands show a clear shift to each other. On average the scenarios with an increase in industrial production show long-term monthly sums of NO_3^--N loads that are 15 tons higher compared to the scenarios with a decrease in industrial production. The same scenarios show larger amplitudes for medium and low NO_3^--N loads, while large NO_3^--N loads remain uninfluenced by the two scenarios for the development of the leather industry.

With the GSA we identified the climate scenarios to have a great influence on all signature measures of the simulated variables. Attributing the uncertainty bands to the individual GCM-RCM combinations unveils diverse outcomes for the future flow regime, the distribution and amplitude of monthly NO_3^--N loads, as well as the appearance of high and low discharges and NO_3^--N loads (Fig. 5). A visual analysis of the separated uncertainty bands identifies the mean annual precipitation anomalies of the GCM-RCM combinations to have a strong impact on the simulation of discharge and NO_3^--N loads. In comparison to the reference period (dashed line), wetter future climate scenarios (blue) simulated larger discharge and NO_3^--N loads, while dryer future conditions lead to a drastic reduction in discharge and NO_3^--N loads.

Half of the 22 implemented GCM-RCM combinations simulated an increase of more than 75 mm (dark blue) and for two GCM-RCM combinations, an increase of more than 25 mm (light blue) of precipitation for the Schwechat catchment was simulated. In contrast, for the Raab nine and four GCM-RCM combinations simulated a decrease in precipitation of more than 75 mm (dark red) and 25 mm (light red), respectively. Consequently, a decrease in discharge and NO_3^--N loads due to a decrease in precipitation is pronounced in the Raab catchment, while the majority of simulations of the Schwechat catchment show an increase in discharge and NO_3^--N loads.

While a grouping of the individual climate scenarios with respect to their temperature anomalies shows a more indefinite picture, all climate scenarios simulated an increase in temperature. Nevertheless, the expectation that an increase in annual mean temperature increases evapotranspiration and thus reduces discharge and NO_3^--N loads is not met in Fig. 6. A clear separation of warmer and cooler climate scenarios, as it is observable for precipitation is not the case with temperature. Consequently, the differences in precipitation predominantly account for the influence of the climate scenarios, rather than the differences in temperature.

Although the influence of the model setups was much lower compared to the influence of the climate scenarios or the model parametrization, the analysis of the uncertainty bands for the different model setups provides interesting insights (Fig. 7). The uncertainty bands do overlap to a great extent, which confirms a low impact of the use of different model setups in the simulation of discharge and NO_3^--N loads. Noteworthy is, that model setups that use the full set of HRUs agree much stronger in their simulations compared to the model setups where the number of HRUs was reduced. The difference between the full HRU and the reduced HRU model setups is distinct in the Schwechat case study. The uncertainty bands of the two full HRU model setups almost completely overlap, although their numbers of subbasins are different (4 and 14 subbasins). The two model setups with a reduced number of HRUs (but also with 4 and 14 subbasins) show differences of up to 15 mm in the simulated monthly specific discharge and up to 7 tons in the monthly NO_3^--N loads (~20 % of the uncertainty bandwidth).
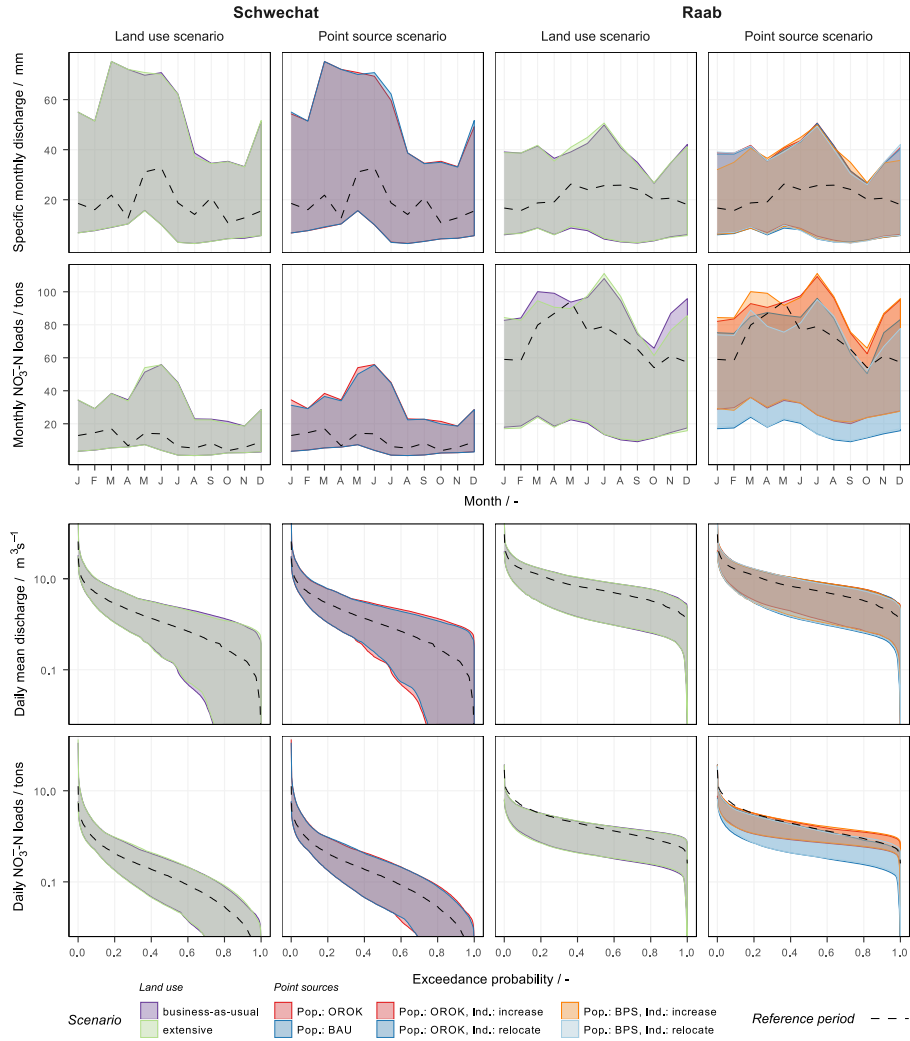
Figure 4. The influence of land use change and the development of point source emissions on the uncertainties resulting from the 7000 combinations of realizations of the influencing variables for the Schwechat (left) and the Raab (right). The uncertainties are illustrated for simulated long-term mean monthly specific discharge (first row), long-term monthly sums of $NO_3^- - N$ loads (second row), FDCs of mean daily discharges (third row), and FDCs for daily sums of $NO_3^- - N$ loads (fourth row). The uncertainty bands are attributed to the implemented land use scenarios (left panels per case study) and the point emission scenarios (right panels). The colors of the grouped uncertainty bands indicate the different scenarios. The dashed lines show the best simulation of the historical reference period. The corresponding land use changes are provided in Table A5. The corresponding population growth scenarios (Pop. in the legend) are listed in Table A6 and the corresponding industrial emission scenarios in the Raab catchment (Ind. in the legend) are listed in Table A7.
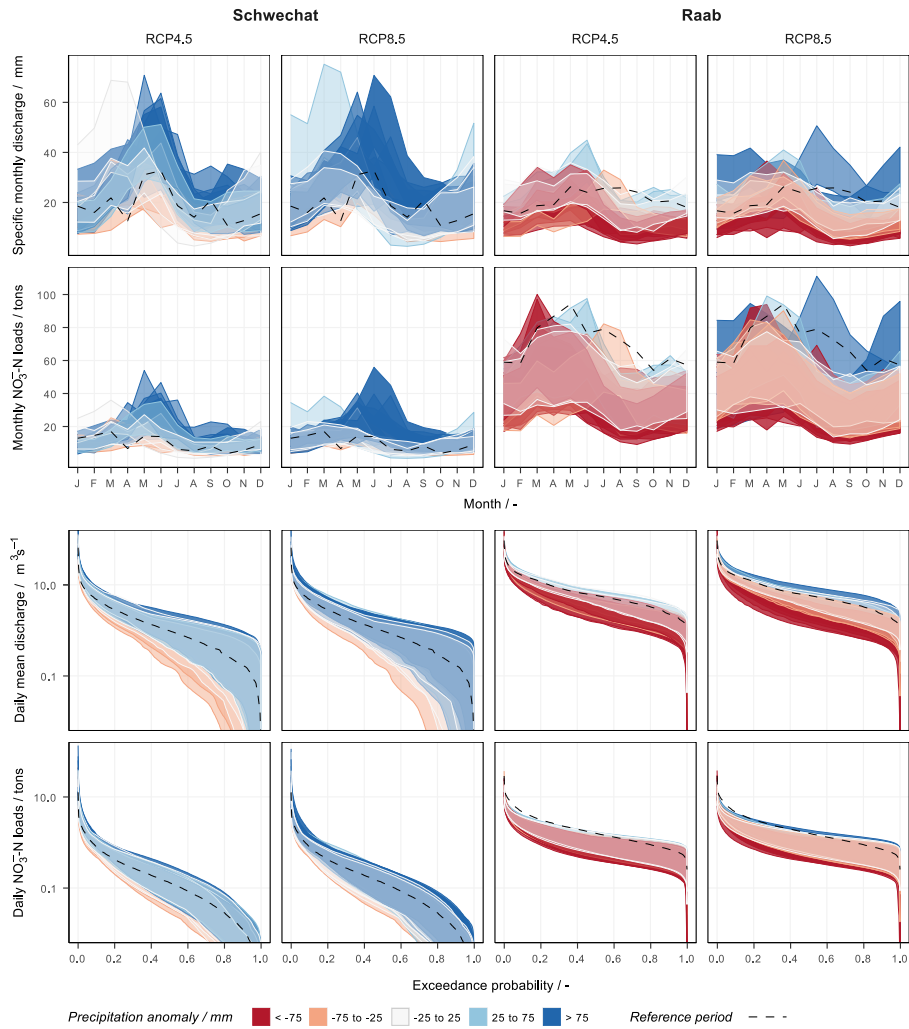
Figure 5. The influence of anomalies in precipitation on the uncertainties resulting from the 7000 combinations of realizations of the influencing variables for the Schwechat (left) and the Raab (right). The uncertainties are illustrated for simulated long-term mean monthly specific discharge (first row), long-term monthly sums of $NO_3^- - N$ loads (second row), FDCs of mean daily discharges (third row), and FDCs for daily sums of $NO_3^- - N$ loads (fourth row). The uncertainty bands are attributed to the individual implemented climate scenarios. The colors of the uncertainty bands show the anomalies in long-term mean annual precipitation of each climate scenario, where blue represents wetter conditions compared to the reference period and red dryer conditions. The dashed lines show the best simulation of the historical reference period.
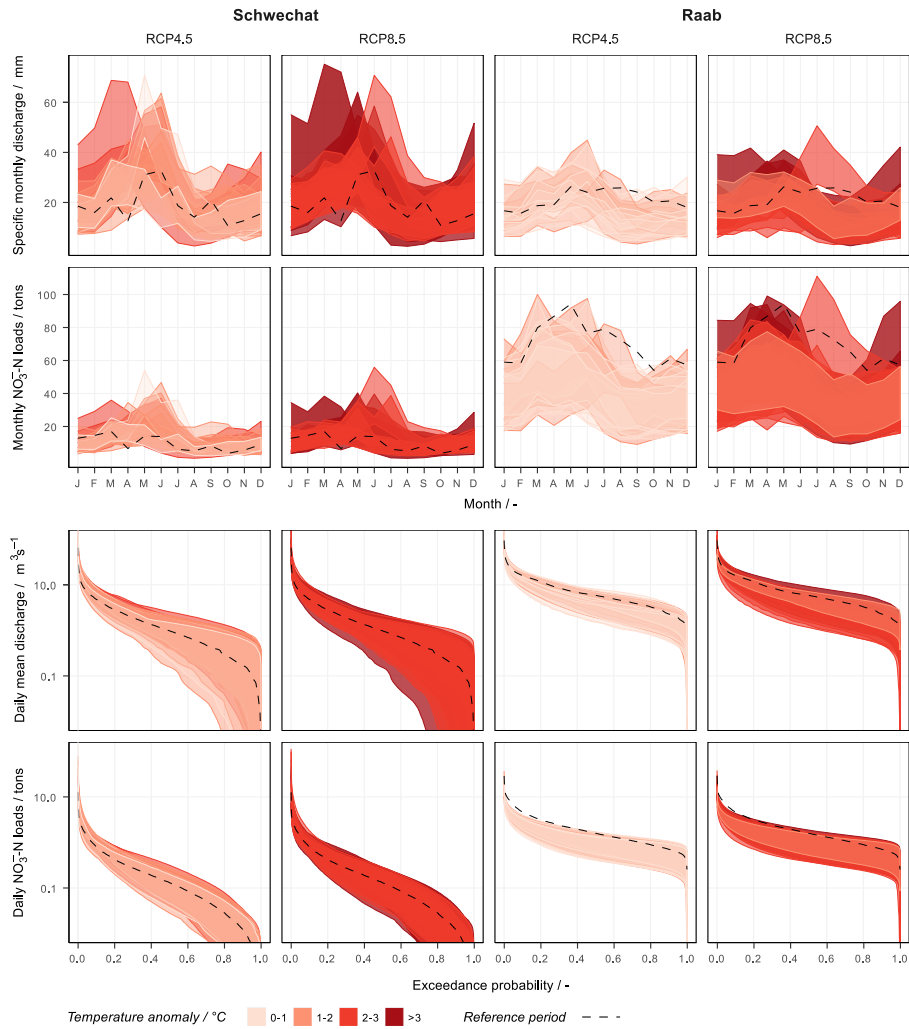
Figure 6. The influence of anomalies in air temperature on the uncertainties resulting from the 7000 combinations of realizations of the influencing variables for the Schwechat (left) and the Raab (right). The uncertainties are illustrated for simulated long-term mean monthly specific discharge (first row), long-term monthly sums of $NO_3^- - N$ loads (second row), FDCs of mean daily discharges (third row), and FDCs for daily sums of $NO_3^- - N$ loads (fourth row). The uncertainty bands are attributed to the individual implemented climate scenarios. The colors of the uncertainty bands show the anomalies in long-term mean annual air temperature of each climate scenario, where a darker red represents hotter conditions compared to the reference period. The dashed lines show the best simulation of the historical reference period.
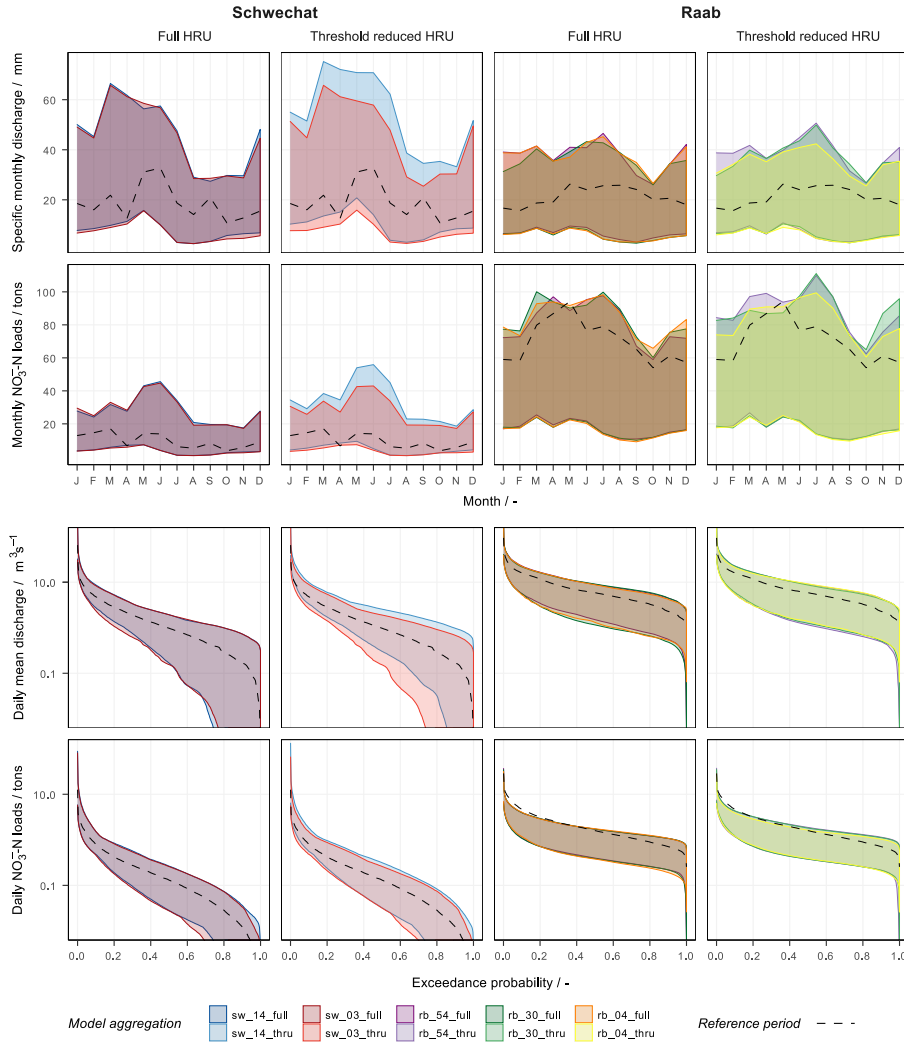
Figure 7. The influence of model setup on the uncertainties resulting from the 7000 combinations of realizations of the influencing variables for the Schwechat (left) and the Raab (right). The uncertainties are illustrated for simulated long-term mean monthly specific discharge (first row), long-term monthly sums of $NO_3^- - N$ loads (second row), FDCs of mean daily discharges (third row), and FDCs for daily sums of $NO_3^- - N$ loads (fourth row). The uncertainty bands are attributed to the individual SWAT model setups. The results are separated for model setups where the full set of HRUs was used (left panels per case study) and for setups with a reduced set of HRUs (right panels). The colors of the uncertainty bands show the different model setups with varying numbers of subbasins. The dashed lines show the best simulation of the historical reference period.

The model parametrizations were relevant for all signature measures of discharge and NO_3^--N loads and were most dominant for medium and low flows. The most dominant model parameters in both case studies were the parameters CNOP_till and SOL_AWC. Both parameters control the water retention and thus the immanent contribution of rainfall to the river discharge. Large values of CNOP_till and small values of SOL_AWC reduce the water retention capacity and increase the amplitude of medium and low discharges (third row in Fig. 8). A similar but inverse behavior is visible with medium NO_3^--N loads (last row in Fig. 8), where a higher water retention results in an increase of NO_3^--N loads. For the long-term monthly mean discharges and sums of NO_3^--N loads two effects are observable in Fig. 8. First, smaller values of CNOP_till and larger values of SOL_AWC decrease the upper boundary of the uncertainty bands. Second, selected model parametrizations with large values of CNOP_till and small values of SOL_AWC cause considerably larger discharges in spring and a strongly reduced runoff in the autumn months in the Schwechat case study.

4   Discussion

4.1   What can we as modelers learn from such analysis

The illustrated case studies emphasized the necessity to characterize, identify and explicitly communicate the uncertainties in a modeling chain, particularly for future simulations of environmental variables where large uncertainties are inherent in several modeling inputs. While the sensitivity analysis of signature measures related to discharge, NO_3^--N loads and NO_3^--N concentrations provided a comprehensive overview of the dominant influencing inputs on specific modeled variables, the analysis of the uncertainty bands for the simulation of the modeled variables provided insights into which properties of the model inputs (e.g. mean annual precipitation or mean air temperature of a climate scenario) control the uncertainties and how these control the simulation. The analyses allow to draw conclusions that are beneficial to consecutive steps of an impact study, for instance to refine the impact study setup and to focus on the most influential components and ultimately to reduce the uncertainties in the modeling simulation chain.

The land use scenarios showed an almost negligible impact on the simulation of discharge and NO_3^--N loads. The discharge and the NO_3^--N loads at the catchment are however integrated signals for the entire catchment and changes in land use may have a greater importance for particular points in a catchment. Many case studies have applied the SWAT model to assess the impact of land use change on different variables of the water cycle (Wagner et al., 2017; Mehdi et al., 2015b), water quality (Guse et al., 2015; Mehdi et al., 2015a), or sediment yield (Bieger et al., 2013). Bieger et al. (2013) found very low land use change induced increases in discharge for a catchment in China. Only an assumed strong intensification of the agriculture led to a 4% increase in discharge. At the same time however, a strong increase in sediment yield of up to 450% for the summer months was simulated due to the intensification of agriculture. Guse et al. (2015) also found only small changes in simulated discharge caused by future land use change in a German lowland catchment. In absolute numbers the simulated future NO_3^--N loads showed small differences between the baseline scenario and the two applied methods of land use change presented by Guse et al. (2015). Yet, the temporal patterns in NO_3^--N loads caused by the different approaches of changing the land use were the major observable difference. Mehdi et al. (2015b) in contrast, found that including future land use change into the impact assessment of a
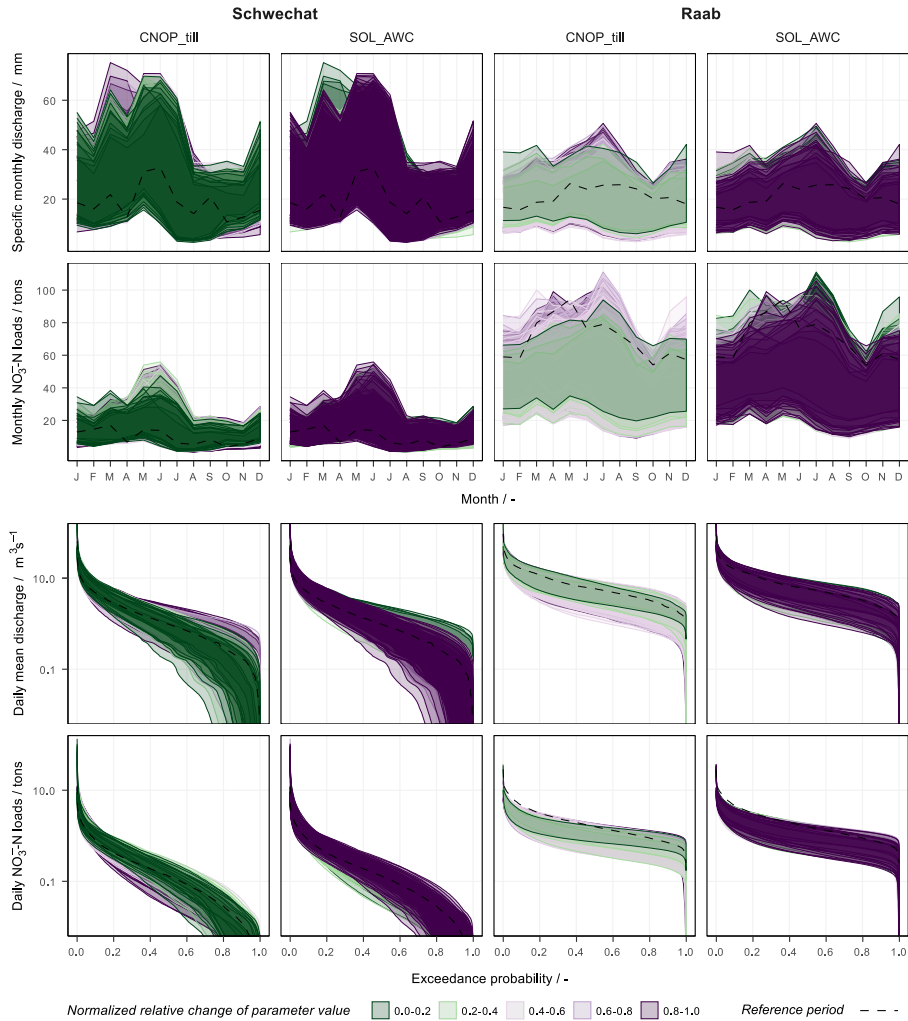
Figure 8. The influence of model parametrization on the uncertainties resulting from the 7000 combinations of realizations of the influencing variables for the Schwechat (left) and the Raab (right). The uncertainties are illustrated for simulated long-term mean monthly specific discharge (first row), long-term monthly sums of $NO_3^- - N$ loads (second row), FDCs of mean daily discharges (third row), and FDCs for daily sums of $NO_3^- - N$ loads (fourth row). The uncertainty bands are attributed to the individual 'behavioral' SWAT model parameter sets. The effect of the two dominant model parameters CNOP_till (left panels for each case study) and SOL_AWC (right panels) is shown. The subsetted uncertainty bands are colored with respect to the changes of the parameter values, shown as normalized values for comparability. The dashed lines show the best simulation of the historical reference period.

southern German watershed strongly increased the NO_3^--N and total phosphorus loads. In comparison, the low impact of land use change found in the present study seems reasonable, particularly as no extreme scenarios were implemented. Nevertheless, an assessment of whether the implemented scenarios adequately reflect the possible futures (e.g. fertilizer management) is recommended.

5   Industrial emitters were the main cause for the impact of point sources on medium to low NO_3^--N loads. The future scenarios of the development of industrial emitters were however highly uncertain. The developed scenarios are based on expert knowledge. Yet, there is no reliable basis available on status of the industrial emitters by the end of the century. Therefore, the developed scenarios should be noted as feasible futures, rather than e.g. politically realizable futures (Godet and Roubelat, 1996). To set a feasible range as boundaries for the future development of industrial emitters can lead to an overestimation

10   of their impact in comparison to other influencing variables. Nevertheless, the visualization of the NO_3^--N FDC of the Raab case study highlights the effect of the industrial emissions for medium and small NO_3^--N loads. Large NO_3^--N loads however, are hardly affected by the implemented scenarios, indicating that large NO_3^--N emissions are mainly driven by agricultural activities.

The selection of climate scenarios had a strong influence on the simulation of discharge and NO_3^--N loads in both case

15   studies. The analysis of the uncertainties bands identified the differences in precipitation between the GCM-RCM combinations as being the main control, while the differences in air temperature had a low impact on the simulation outcome. This finding stands in contrast to other studies. Milly and Dunne (2011) and Sheffield et al. (2012) for example, identified empirical approaches for the calculation of evapotranspiration as the main source for overestimation of the climate's influence on hydrological processes, particularly when evapotranspiration is a function of air temperature (Clark et al., 2016; Shaw and

20   Riha, 2011; Roderick et al., 2014). In the climate scenarios used in this study, the impact of large differences in mean annual precipitation on the simulated outputs exceeded the impact of the differences in air temperature.

The effect of the model setup, with different watershed subdivisions, on the simulation of discharge or water quality variables has been investigated in various studies (e.g. Jha et al., 2004; Momm et al., 2017; Pignotti et al., 2017). Jha et al. (2004) emphasize the greater impact of changes during the HRU definition over the defined number of subbasins, as a consequent

25   change in the distribution of land use, soil, or topography strongly affect runoff and the nutrient budget in a catchment. The analysis of the uncertainties bands with respect to the different model setups clearly confirmed the study by Jha et al. (2004), especially in the case of the Schwechat. Nevertheless, the impact of the model setup was lower than the effect of the model parametrization by a factor of up to five in the Schwechat study and up to eight in the Raab case study. Yet, the model setup strongly affects the computation time. In the present case, where aggregated discharge and NO_3^--N loads at the catchment

30   outlets were the variables of interest a strong focus on the model parametrization is of higher priority than the spatial distribution of the model setup. Therefore, to maintain short computation times (and at the same time to maintain the distributions of land use, soil, or topography) a model setup with a low number of subbasins without any reduction of the number of HRUs is beneficial.

The impact of parameter non-uniqueness on the simulation of hydrological and water quality variables has been demon-

35   strated previously (e.g.; Wilby, 2005; Mehdi et al., 2018). The importance of the model parametrization for the simulation

of discharge and NO_3^--N loads was confirmed in the present study as well. Large sensitivities of all signature measures of discharge and NO_3^--N loads to the different model parametrizations were identified . Although all selected parameter sets represented historical observations of discharge and NO_3^--N loads with a certain goodness of fit (based on defined objective criteria), the colored grouping of the uncertainty bands illustrated that the selected model parameter sets control the simulation

5 of future discharge and NO_3^--N loads in different ways. Thus, the large impact of the model parametrization and the distinctive patterns identified in the uncertainty bands suggest a great potential to further refine the model parametrization and consequently reduce simulation uncertainties with a more intensive model calibration. Additional information on the time series of observations can help to constrain the model parameters and adequately describe the relevant processes (e.g. Hrachowitz et al., 2014; Pfannerstill et al., 2017).

10 **4.2   How to attribute subjectivity inherent in the scenarios**

Scenarios always reflect subjective assumptions made by the modeler. Assumptions that are made in the scenario development however, can strongly influence a simulation and thus affects a comparison of different model inputs and their impacts on the simulation. All steps in a scenario development involve subjective assumptions and can lack plausibility (Mahmoud et al., 2009; van Vuuren et al., 2012), regardless of whether the process involves expert knowledge, the input of stakeholders in an

15 participatory process, or an exploratory approach that extrapolates trends, these practices potentially introduce uncertainties in the definition of scenarios. Technical aspects such as how the scenario is represented in the model are also strongly biased by the modelers decision and represent an additional source of uncertainty (Mahmoud et al., 2009). The communication of the potential uncertainties inherent in the developed scenarios and the boundaries of the explanatory power of an scenario ensemble is essential for the integrity of any impact study (Mahmoud et al., 2009; Jones et al., 2014).

20   In the present study, several assumptions were made in the development of scenarios that are highly subjective, such as the extrapolated gradient of future land use changes, the drastic changes in future industrial emissions, and also the selection of objective criteria that define a behavioral SWAT model setup. Scenarios must cover a broad range of possible futures and have to be adequately represented in the model setup. An explicit delineation of the implemented scenarios and their limitations is essential to clearly illustrate the limitations of an impact study's conclusions. An immanent risk in any impact study is that

25 the model representation of a future change, or the uncertainties in a model input fail to reproduce the response of a simulated variable that would have taken place in the real environmental system. Hence, a detailed analysis of the simulation uncertainties perfectly complements a SA to identify possible shortcomings in the study setup. Attributing the uncertainty bands resulting from the simulation of an environmental variable to individual model inputs prove to be a useful visual analysis tool that gives the power to illustrate the uncertainties in a transparent way. Furthermore, the colored differentiation provides a visual guidance

30 to judge the impacts of different implemented scenarios.

4.3   Sensitivity analysis or hydrologic storylines

The presented approach implements large samples combining scenarios for different model inputs and different model setups and parametrizations in a GSA to identify the dominant contributors of uncertainties in the simulated outputs. The utilization

of SA with large sample sizes however, raises the following issues: i) compared to a standard approach to perform an impact assessment, where a few different future scenarios are implemented into a model, the computational demand of a GSA requiring hundreds or thousands of model executions is larger by several orders of magnitude. Thus, a practical implementation of the presented procedure in impact studies is questionable and a strong cooperation between research and the practitioners

5   is essential. ii) scenarios of different model inputs are often interrelated (Mahmoud et al., 2009). A change in one model input therefore for example expects the change of another model input into one direction and makes a change into another direction unlikely. While the implementation of input dependencies, althouh challenging is feasible for continuous model inputs, for instance by a transformation of the input space (e.g., Tarantola and Mara, 2017; Mara and Tarantola, 2012), or the determination of input distribution functions (Hart and Gremaud, 2018), the dependencies of composite model inputs are

10   usually difficult to express mathematically. To identify the dependencies between composite model inputs, expert knowledge is required to properly constrain the model input combinations and therefore complicates the implementation in approaches, such as the presented one.

Clark et al. (2016) therefore suggest to identify consistent hydrologic story lines that result in least severe, most likely, and most severe responses of the modeled system. Such an approach would tremendously reduce the number of necessary

15   model evaluations, but also establish consistency between the considered influencing variables. Nevertheless, the feasible combinations of influencing variables that lead to extreme or likely responses of the modeled system are hardly known a priori. Consequently, a sensitivity analysis with a constrained sampling space, to avoid infeasible combinations of influencing variables might be a pragmatic compromise.

5   Conclusions

20   In this study we utilized methods for GSA in environmental impact studies to identify the dominant sources of uncertainties for the simulation of environmental variables under future changing conditions. In two Austrian case studies for the rivers Schwechat and Raab, we simulated the river discharge and the NO_3^--N loads from the catchments under the condition of future changes in climate, land use, and emissions from urban and industrial point sources implementing different SWAT model setups with various model parametrizations.

25   Both case studies identified climate change and the model parametrization to be the most important (influential) model inputs for the simulation of discharge and NO_3^--N loads, based on performing a GSA and on the resulting analysis of signature measures of discharge and NO_3^--N loads (quantiles of discharge and NO_3^--N loads, seasonal mean discharge and seasonal sums of NO_3^--N loads and NO_3^--N concentrations for discharge quantiles). The impact of the model setup on simulated variables of discharge and NO3-N loads was found to be considerably lower than the impact of the model parametrization

30   for the Schwechat and even more distinct for the Raab. The impact of the implemented scenarios for land use and municipal point source emissions were negligible for all analyzed signature measures. Because of a large leather industry in the Raab catchment, the future development of industrial emission in the Raab catchment was found to be relevant for low NO_3^--N loads and NO_3^--N concentrations during low discharge.

Accompanying the GSA, a detailed analysis of the simulation uncertainties provided additional insights on how the uncertainties in the model inputs control simulated discharge and NO_3^--N loads. The visualizations we developed proved to be an effective tool to identify the relevant properties of the model inputs that control the simulation uncertainties and provide insight how individual realizations of a model input can affect the simulations. In the climate simulations, we found the precipitation to dominate the simulation outputs, rather than changes in air temperature. Although the impact of the model setup on the simulation of discharge and NO_3^--N loads was low, the visual analysis of the uncertainty bands illustrated that the HRU definition is an important step in the model setup. The use of the full set of HRUs was identified as the preferred setup in the two case studies. In contrast the effect of using different numbers of subbasins in the model setup was low for the simulation of discharge and NO_3^--N loads at the catchment outlets.

The drawn conclusions are the result of specific conditions and the assumptions made for each individual catchment in the two case studies. The conclusions cannot be extrapolated with ease to other catchments. Nevertheless, the presented work provides an approach to identify and analyze the dominant sources of simulation uncertainties in environmental impact studies that can easily be generalized and that can act as a template for further impact studies. The analyses advocate for a stronger focus on the communication of uncertainties in model simulation and their sources in environmental impact studies. Although a variety of tools to perform SA are available for different programming languages (e.g., Pianosi and Wagener, 2015; Reusser, 2015; Iooss et al., 2018; Houska et al., 2015), the main constraint for a practical application remains the development of a comprehensive set of discrete input realizations, the computational costs of such analysis, and the lack if straight forward methods to implement composite inputs into SA. This might detain the practical application of such methods. To facilitate the implementation of composite model inputs in SA, we plan to implement the demonstrated procedures and tools for visualization into a user friendly programming environment.

Appendix A: Supplementary figures and tables
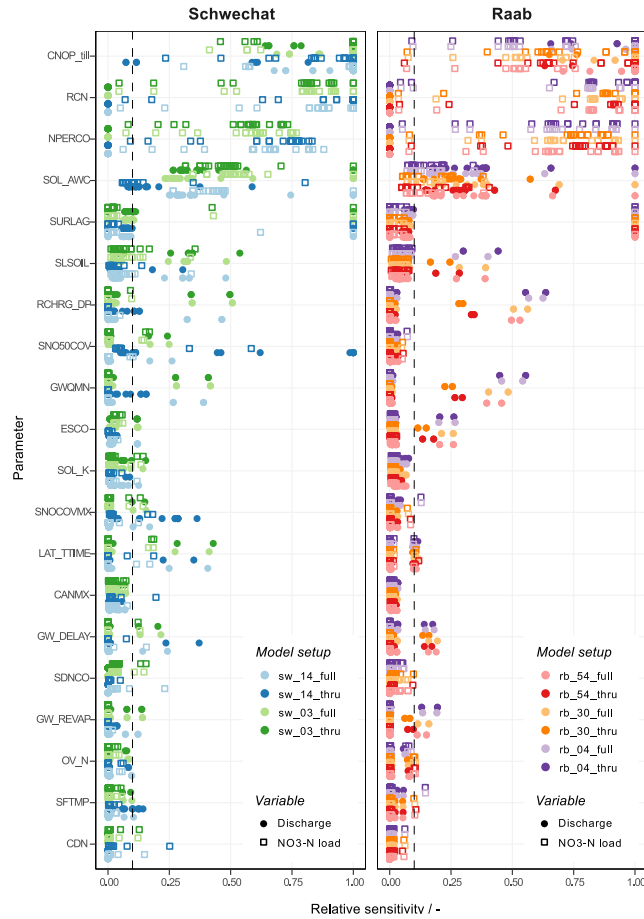
Figure A1. Identification of the influential SWAT model parameters for the case studies Schwechat (left) and Raab (right). The y-axis illustrates model parameters that showed an impact on at least one of the analyzed objective criteria. The x-axis shows the relative sensitivities of analyzed objective criteria (in relation to the most influential parameter for an objective criterion). The colors indicate the different SWAT model setups. The circles show the sensitivities for objective criteria related to discharge, while the hollow squares show parameter sensitivities for $NO_3^- - N$ loads. The dashed line indicates the 0.1 value of relative sensitivity. A parameter is considered to be sensitive if it resulted in a relative sensitivity above this threshold for the objective criteria.
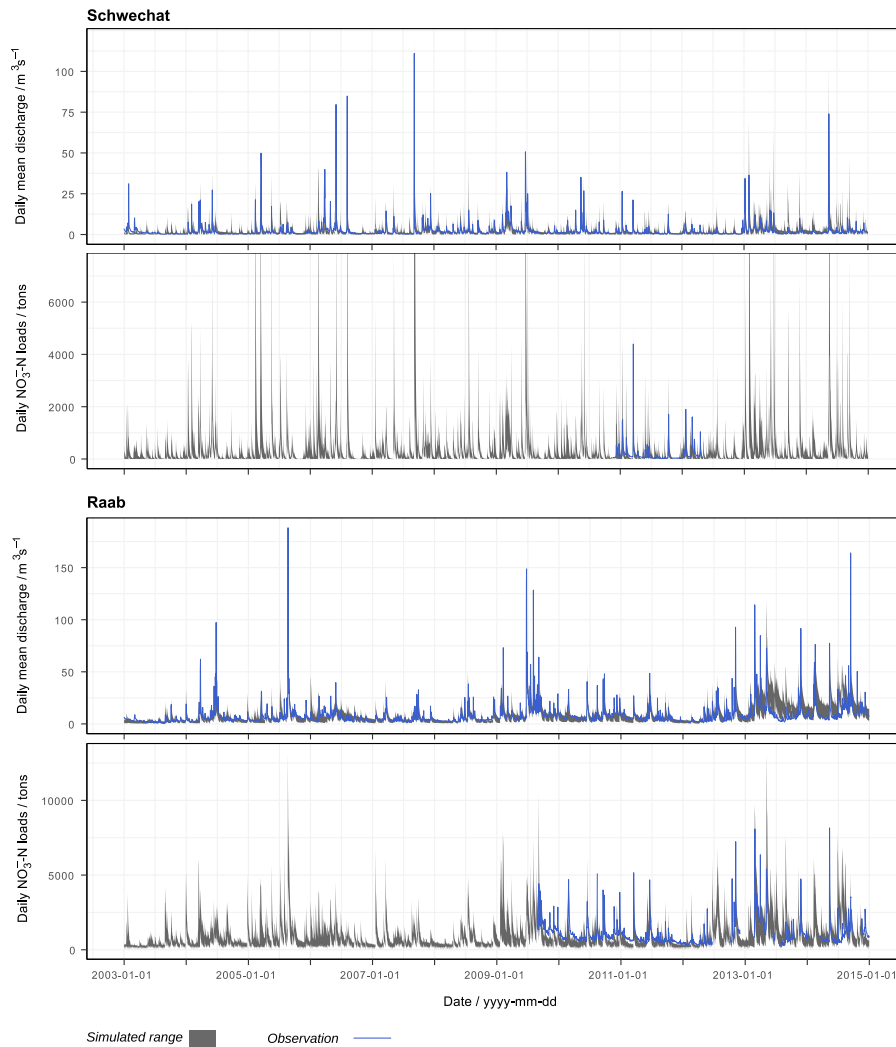
Figure A2. Simulated time series of daily mean discharge and daily $NO_3^- - N$ loads for the Schwechat (top) and the Raab (bottom) catchments for the time period 2003 to 2015. The gray bands show the ranges simulated using the selected model parameter sets with the different SWAT model setups. The blue solid lines indicate available observations of discharge and $NO_3^- - N$ loads for the respective time periods.

Catchment • Schwechat • Raab
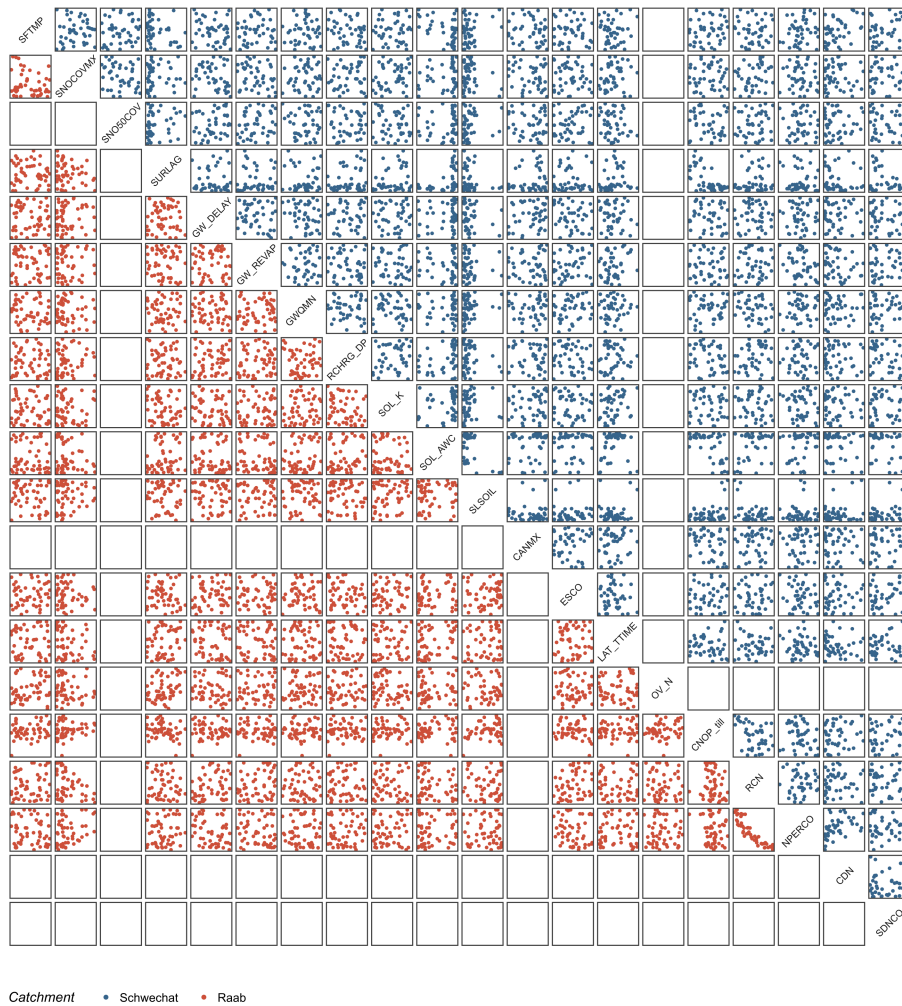
Figure A3. Parallel coordinate plot of the 43 and 52 behavioral SWAT model parameter combinations that were used with the model setups of the Schwechat and the Raab, respectively. Each panel illustrates the interaction of two model parameters. The parameter combinations for the Schwechat are illustrated in red (below the diagonal) and the combinations for the Raab are given in blue (above the diagonal). The x and y axes of each panel show the range of the respective parameter plotted along the x or y dimension. The corresponding parameter ranges for all illustrated parameters are provided in Table A2.

Table A1. Sensitive SWAT model parameters for the model setups of the Schwechat and the Raab.

Parameter	Description	Influential for discharge		Influential for NO$_3^-$-N loads	
		Schwechat	Raab	Schwechat	Raab
SFTMP	Snowfall temperature (°C)	X			X
SNOCOVMX	Minimum snow water content that corresponds to 100% snow cover	X		X	X
SNO50COV	Snow water equivalent that corresponds to 50% snow cover	X		X	
SURLAG	Surface runoff lag time (h)	X	X	X	X
GW_DELAY	Groundwater delay (d)	X	X	X	
GW_REVAP	Groundwater revaporation coefficient	X	X		
GWQMN	Threshold depth of water in shallow aquifer for return flow (mm)	X	X		
RCHRG_DP	Deep aquifer percolation fraction	X	X		
SOL_K	Saturated hydraulic conductivity (mm/h)	X		X	
SOL_AWC	Available water capacity of the soil layer	X	X	X	
SLSOIL	Slope length for lateral subsurface flow	X	X	X	X
CANMX	Maximum canopy storage			X	
ESCO	Soil evaporation compensation factor	X	X		
LAT_TTIME	Lateral flow travel time	X	X	X	X
OV_N	Manning's n-value for overland flow		X		X
CNOP_till	SCS runoff curve number for the tillage operation	X	X	X	X
RCN	Concentration of nitrogen in rainfall			X	X
NPERCO	Nitrogen percolation coefficient			X	X
CDN	Denitrification exponential rate coefficient			X	
SDNCO	Denitrification threshold water content			X	

Table A2. Ranges of parameter changes for the behavioral model parameter sets. The type of change indicates whether a model parameter was replaced by absolute values, altered by adding an absolute to the initial parameter value, or changed by a relative fraction of the initial parameter value. The initial ranges of parameter changes and the ranges of parameter ranges of the behavioral parameter combinations in the model setups of the Schwechat and the Raab are shown.

Parameter	Type of change	Range of parameter change		
		Initial range	Schwechat	Raab
SFTMP	replace value	[-1.00, 1.00]	[-0.69, 0.93]	[-0.98, 0.88]
SNOCOVMX	replace value	[100.0, 500.0]	[0.9, 177.0]	[100.8, 447.5]
SNO50COV	replace value	[0.20, 0.50]	[0.21, 0.49]	
SURLAG	replace value	[0.00, 18.00]	[0.02, 0.99]	[0.01, 0.10]
GW_DELAY	replace value	[0.0, 300.0]	[5.5, 25.0]	[2.1, 283.3]
GW_REVAP	replace value	[0.02, 0.20]	[0.05, 0.15]	[0.02, 0.20]
GWQMN	replace value	[0, 3000]	[567, 2472]	[109, 2925]
RCHRG_DP	replace value	[0.01, 1.00]	[0.31, 0.69]	[0.13, 0.97]
SOL_K	relative change	[-0.90, 10.00]	[0.00, 0.97]	[-0.79, 9.76]
SOL_AWC	relative change	[-0.90, 2.00]	[-0.86, 1.49]	[0.01, 1.98]
SLSOIL	replace value	[0.0, 150.0]	[0.9, 27.6]	[14.7, 148.2]
CANMX	relative change	[-0.90, 2.50]	[0.34, 2.40]	
ESCO	replace value	[0.00, 0.90]	[0.05, 0.9]	[0.05, 0.89]
LAT_TTIME	replace value	[0.0, 180.0]	[0.8, 6.8]	[5.5, 176.3]
OV_N	absolute change	[-0.09, 0.60]		[0.07, 0.58]
CNOP_till	relative change	[-0.20, 0.10]	[-0.19, -0.06]	[-0.18, 0.01]
RCN	replace value	[2.00, 10.00]	[5.05, 9.97]	[2.30, 8.45]
NPERCO	replace value	[0.00, 1.00]	[0.24, 0.99]	[0.18, 0.7]
CDN	replace value	[0.00, 1.50]	[0.01, 1.44]	
SDNCO	replace value	[0.00, 0.50]	[0.02, 0.49]	

Table A3. Area and percentage of the land uses in the Schwechat catchment. The land use groups are the respective land uses shown in Fig. 1 and are derived from CORINE. With a higher thematic resolution the land uses that were implemented in the SWAT models are listed providing their areas and their percentages in the catchment.

Land use group	CORINE Level 3	Land use	SWAT Land use	Area / ha	Percentage / %
Urban/Industrial	11X, 14X	Urban medium density	URMD	154.2	0.6
	11X, 14X	Urban medium/low density	URML	2388.3	8.7
	12X	Industrial	UIDU	209.5	0.8
Agriculture, Complex Cultiv.	221, 222, 242	Winter wheat, winter grains	WWHT	667.6	2.4
		Spring wheat, summer grains	SWHT	317.8	1.2
		Corn, Maize	CORN	111.5	0.4
		Vegetables grouped	SGBT	74.1	0.3
		Sunflower	SUNF	30.0	0.1
		Soybean	SOYB	19.7	0.1
		Orchard, Fruit trees	ORCD	25.6	0.1
		Vineyard	GRAP	699.5	2.5
Grassland, Complex Cultiv.	231, 242	Pasture, extensive use	FESC	2406.6	8.8
		Pasture, intensive use	FESI	762.9	2.8
		Alfalfa, clover, etc.	ALFA	400.7	1.5
Deciduous forest	311	Forest, deciduous	FRSD	12941.3	47.1
Coniferous forest	312	Forest evergreen	FRSE	1152.2	4.2
Mixed forest	312	Forest, mixed	FRST	5138.4	18.7
				27499.9	100.0

Table A4. Area and percentage of the land uses in the Raab catchment. The land use groups are the respective land uses shown in Fig. 1 and are derived from CORINE. With a higher thematic resolution the land uses that were implemented in the SWAT models are listed providing their areas and their percentages in the catchment.

Land use group	CORINE Level 3	Land use	SWAT Land use	Area / ha	Percentage / %
Urban/Industrial	11X, 14X	Urban medium/low density	URML	11850.8	12.0
Agriculture, Complex Cultivation	221, 222, 242	Corn, Maize	CORN	11982.5	12.1
		Oil seed pumpkin	OELK	3171.1	3.2
		Vegetables grouped	SGBT	3035.9	3.1
		Winter wheat, winter grains	WWHT	1855.6	1.9
		Spring wheat, summer grains	WWHT	981.9	1.0
		Soybean	SOYB	445.9	0.5
		Orchard, fruit trees	ORCD	3036.1	3.1
Grassland, Complex Cultivation	231, 242	Pasture, extensive use	FESC	11635.7	11.8
		Pasture, intensive use	FESI	8474.0	8.6
		Alfalfa, clover, etc.	ALFA	598.0	0.6
Deciduous forest	311	Forest, deciduous	FRSD	15379.4	15.6
Coniferous forest	312	Forest evergreen	FRSE	7773.2	7.9
Mixed forest	312	Forest, mixed	FRST	18540.2	18.8
Waterbodies	41X	Wetlands, mixed	WETL	55.4	0.1
				98815.9	100.0

Table A5. Transformations of land uses (LUSE) in the implemented land use scenarios at the Schwechat and the Raab.

| | "business-as-usual" | | | "extensive" | |
From LUSE	To LUSE	Change %/ha	From LUSE	To LUSE	Change %/ha
Schwechat:					
Urban, light	Urban, dense	10 / 239	Winter wheat	Ext. pasture	27.5 / 184
Ext. pasture	Urban, light	15 / 361	Winter wheat	Legumes	27.5 / 184
Ext. pasture	Winter wheat	20 / 481			
Raab:					
Ext. pasture	Corn	75 / 8726	Corn	Ext. pasture	27.5 / 3595
Sugar beet	Corn	80 / 2429	Corn	Legumes	27.5 / 3595
Legumes	Corn	70 / 419			
Winter wheat	Corn	30 / 557			

Table A6. Municipal point source emissions and changes in the emissions due to different population growth scenarios in the Schwechat and the Raab catchments.

District	Scenario BAU/BPS			Scenario OROK		
	Change / %	Population	NO_3^--N / $kg \cdot yr^{-1}$	Change / %	Population	NO_3^--N / $kg \cdot yr^{-1}$
Baden (Schwechat)	0.0	32058	39842	+32.0	42317	52591
Total Schwechat	0.0	32058	39842	+32.0	42317	52591
Weiz (Raab)	+7.7	56982	44918	-2.0	51529	40872
Südoststeiermark (Raab)	+2.3	32296	16537	-20.4	25117	12868
Total Raab	+5.7	89278	61455	-8.7	76646	53740

Table A7. Industrial point source emissions and implemented changes in the emissions at the Raab due to increase in production or relocation of the dominant leather producer.

Industrial emitter	Relocation of leather industry		Increase in production	
	Change / %	NO_3^--N / $kg \cdot yr^{-1}$	Change / %	NO_3^--N / $kg \cdot yr^{-1}$
Agrana Fruit Austria GmbH	0.0	1029	0.0	1029
BOXMARK Leder/Feldbach	-100.0	0	30.0	88257
BOXMARK Leder/Jennersdorf	-100.0	0	30.0	36442
Fleischhof Raabtal GmbH	0.0	292	0.0	292
Johann Titz GmbH	0.0	3774	0.0	3774
WOLLSDORF Leder	0.0	26572	0.0	26572
Total	-75.20	31667	22.6	156366

Table A8. GCM-RCM combinations implemented in the study with their long-term mean annual precipitation sums and long-term mean annual temperatures for the Schwechat and the Raab.

Model	Schwechat		Raab	
	$P\,/\,mm \cdot yr^{-1}$	$T\,/\,°C$	$P\,/\,mm \cdot yr^{-1}$	$T\,/\,°C$
EUR-11_CNRM-CERFACS-CNRM-CM5_RCP45_CLMcom-CCLM4-8-17	845.6	10.5	1103.0	12.4
EUR-11_CNRM-CERFACS-CNRM-CM5_RCP85_CLMcom-CCLM4-8-17	828.7	11.6	1075.6	13.7
EUR-11_CNRM-CERFACS-CNRM-CM5_RCP45_SMHI-RCA4	911.9	10.9	1118.0	12.6
EUR-11_CNRM-CERFACS-CNRM-CM5_RCP85_SMHI-RCA4	943.8	12.4	1091.0	14.4
EUR-11_ICHEC-EC-EARTH_RCP45_CLMcom-CCLM4-8-17	813.3	10.6	967.0	12.5
EUR-11_ICHEC-EC-EARTH_RCP85_CLMcom-CCLM4-8-17	809.2	12.1	941.5	14.4
EUR-11_ICHEC-EC-EARTH_RCP45_SMHI-RCA4	915.8	11.2	1018.4	12.9
EUR-11_ICHEC-EC-EARTH_RCP85_SMHI-RCA4	939.7	12.9	1036.1	15.1
EUR-11_ICHEC-EC-EARTH_RCP45_KNMI-RACMO22E	772.7	10.9	965.0	12.6
EUR-11_ICHEC-EC-EARTH_RCP85_KNMI-RACMO22E	779.0	12.6	925.6	14.6
EUR-11_ICHEC-EC-EARTH_RCP45_DMI-HIRHAM5	925.8	10.4	962.8	12.4
EUR-11_ICHEC-EC-EARTH_RCP85_DMI-HIRHAM5	912.9	12.1	976.8	14.4
EUR-11_IPSL-IPSL-CM5A-MR_RCP45_IPSL-INERIS-WRF331F	907.2	10.2	1046.7	13.0
EUR-11_IPSL-IPSL-CM5A-MR_RCP85_IPSL-INERIS-WRF331F	996.2	11.6	1202.2	14.6
EUR-11_IPSL-IPSL-CM5A-MR_RCP45_SMHI-RCA4	899.8	11.7	1076.8	13.7
EUR-11_IPSL-IPSL-CM5A-MR_RCP85_SMHI-RCA4	934.6	13.5	1217.3	15.9
EUR-11_MPI-M-MPI-ESM-LR_RCP45_CLMcom-CCLM4-8-17	839.1	11.5	960.5	13.6
EUR-11_MPI-M-MPI-ESM-LR_RCP85_CLMcom-CCLM4-8-17	867.9	13.3	913.2	15.7
EUR-11_MOHC-HadGEM2-ES_RCP45_SMHI-RCA4	974.4	11.6	1108.5	13.6
EUR-11_MOHC-HadGEM2-ES_RCP85_SMHI-RCA4	945.0	13.6	1117.4	15.9
EUR-11_MOHC-HadGEM2-ES_RCP45_SMHI-RCA4	781.1	10.2	940.3	12.2
EUR-11_MOHC-HadGEM2-ES_RCP85_SMHI-RCA4	813.2	12.0	1021.4	14.3

Author contributions. Christoph Schürz, Bano Mehdi, and Karsten Schulz contributed in the development of the study framework and prepared the manuscript. Christoph Schürz designed and performed all analyses illustrated in the paper. Bano Mehdi and Christoph Schürz developed the land use change scenarios, Brigitta Hollosi and Christoph Matulla developed the climate scenarios, and Alexander Pressl and Thomas Ertl calculated present wastewater emissions and developed the future municipal and industrial emission scenarios.

5   *Competing interests.* The authors declare no competing interests.

Acknowledgements. This work is a result from the project UnLoadC^3 (Project No.: KR13AC6K11021) funded by the Austrian Climate and Energy Fund in the 6th call of the ACRP program line. We gratefully obtained time series data of NO_3^--N concentration from Stefan Schuster (TBS Water Consult) and Roland Fuiko (IWR TU Wien) who manage the Raab monitoring data at the Stations Takern II and Neumarkt a.d. Raab. We want to thank Francesca Pianosi, Björn Guse, and the two anonymous reviewers for their detailed comments that

10   helped to substantially improve the paper.

References

Amt d. Stmk LReg: Regionale Bevölkerungsprognose Steiermark 2015/16 -Bundesland, Bezirke und Gemeinden, Tech. rep., Graz, Austria, http://docplayer.org/32447223-Regionale-bevoelkerungsprognose-steiermark-2015-16-bundesland-bezirke-und-gemeinden.html, 2016.

Anderson, B., Borgonovo, E., Galeotti, M., and Roson, R.: Uncertainty in climate change modeling: can global sensitivity analysis be of help?, Risk analysis, 34, 271–293, https://doi.org/10.1111/risa.12117, 2014.

Arnold, J. G., Srinivasan, R., Muttiah, R. S., and Williams, J. R.: Large area hydrologic modeling and assessment part I: model development, Journal of the American Water Resources Association, 34, 73–89, https://doi.org/10.1111/j.1752-1688.1998.tb05961.x, 1998.

Baroni, G. and Tarantola, S.: A General Probabilistic Framework for uncertainty and global sensitivity analysis of deterministic models: A hydrological case study, Environmental Modelling & Software, 51, 26–34, https://doi.org/10.1016/j.envsoft.2013.09.022, 2014.

Beven, K.: The limits of splitting: Hydrology, Science of the Total Environment, 183, 89–97, https://doi.org/10.1016/0048-9697(95)04964-9, 1996.

Beven, K.: A manifesto for the equifinality thesis, Journal of Hydrology, 320, 18–36, https://doi.org/10.1016/j.jhydrol.2005.07.007, 2006.

Beven, K. and Freer, J.: Equifinality, data assimilation, and uncertainty estimation in mechanistic modelling of complex environmental systems using the GLUE methodology, Journal of Hydrology, 249, 11 – 29, https://doi.org/https://doi.org/10.1016/S0022-1694(01)00421-8, 2001.

BGBl. 1996/210: Verordnung des Bundesministers für Land- und Forstwirtschaft über die Begrenzung von Abwasseremissionen aus Abwasserreinigungsanlagen für Siedlungsgebiete (1. AEV für kommunales Abwasser), 1996.

BGBl. II 2006/96: Qualitätszielverordnung Chemie Oberflächen-gewässer (QZV Chemie OG), 2006.

BGBl. II 2010/99: Qualitätszielverordnung Ökologie Oberflächen-gewässer (QZV Ökologie OG), 2010.

BGBl. II Nr. 10/1999: Verordnung des Bundesministers für Land- und Forstwirtschaft über die Begrenzung von Abwasseremissionen aus Gerbereien, Lederfabriken und Pelzzurichtereien (AEV Gerberei), 1999.

BGBl. II Nr. 12/1999: Verordnung des Bundesministers für Land- und Forstwirtschaft über die Begrenzung von Abwasseremissionen aus der Schlachtung und Fleischverarbeitung (AEV Fleischwirtschaft), 1999.

Bieger, K., Hörmann, G., and Fohrer, N.: The impact of land use change in the Xiangxi Catchment (China) on water balance and sediment transport, Regional Environmental Change, 15, 485–498, https://doi.org/10.1007/s10113-013-0429-3, 2013.

BMLFUW: IMW3: Integrierte Betrachtung eines Gewässerabschnitts auf Basis kontinuierlicher und validierter Langzeitmessreihen [Integrated Monitoring of a river section on the basis of continuous and validated long measurement time series] (In German), Tech. rep., Bundesministerium für Land- und Forstwirtschaft, Umwelt und Wasserwirtschaft, Sektion VII Wasser, Vienna, 2013.

BMLFUW: Online monitoring at the Station Neumarkt/Raab at the River Raab. Operated by the TU Wien, Institut für Gewässergüte, Resourcenmanagement und Abfallwirtschaft, 2015a.

BMLFUW: Online monitoring at the Station St.Margarethen/Takern II at the River Raab. Operated by TBS Water Consult., 2015b.

Borgonovo, E., Lu, X., Plischke, E., Rakovec, O., and Hill, M. C.: Making the most out of a hydrological model data set: Sensitivity analyses to open the model black-box, Water Resources Research, pp. 7933–7950, https://doi.org/10.1002/2017WR020767, 2017.

Butler, M. P., Reed, P. M., Fisher-Vanden, K., Keller, K., and Wagener, T.: Identifying parametric controls and dependencies in integrated assessment models using global sensitivity analysis, Environmental modelling & software, 59, 10–29, https://doi.org/10.1016/j.envsoft.2014.05.001, 2014.

Canty, A. and Ripley, B. D.: boot: Bootstrap R (S-Plus) Functions, r package version 1.3-20, 2017.

Chiew, F. H. and Vaze, J.: Hydrologic nonstationarity and extrapolating models to predict the future: Overview of session and proceeding, in: IAHS-AISH Proceedings and Reports, vol. 371, pp. 17–21, https://doi.org/10.5194/piahs-371-17-2015, 2015.

Clark, M. P., Slater, A. G., Rupp, D. E., Woods, R. A., Vrugt, J. A., Gupta, H. V., Wagener, T., and Hay, L. E.: Framework for Understanding Structural Errors (FUSE): A modular framework to diagnose differences between hydrological models, Water Resources Research, 44, https://doi.org/10.1029/2007WR006735, 2008.

Clark, M. P., Wilby, R. L., Gutmann, E. D., Vano, J. A., Gangopadhyay, S., Wood, A. W., Fowler, H. J., Prudhomme, C., Arnold, J. R., and Brekke, L. D.: Characterizing Uncertainty of the Hydrologic Impacts of Climate Change, Current Climate Change Reports, 2, 55–64, https://doi.org/10.1007/s40641-016-0034-x, 2016.

Cuntz, M., Mai, J., Zink, M., Thober, S., Kumar, R., Schäfer, D., Schrön, M., Craven, J., Rakovec, O., Spieler, D., Prykhodko, V., Dalmasso, G., Musuuza, J., Langenberg, B., Attinger, S., and Samaniego, L.: Computationally inexpensive identification of noninformative model parameters by sequential screening, Water Resources Research, 51, 6417–6441, https://doi.org/10.1002/2015WR016907, 2015.

Dai, H. and Ye, M.: Variance-based global sensitivity analysis for multiple scenarios and models with implementation using sparse grid collocation, Journal of Hydrology, 528, 286–300, https://doi.org/10.1016/j.jhydrol.2015.06.034, 2015.

Dai, H., Ye, M., Walker, A. P., and Chen, X.: A new process sensitivity index to identify important system processes under process model and parametric uncertainty, Water Resources Research, 53, 3476–3490, https://doi.org/10.1002/2016WR019715, 2017.

Dile, Y. T., Daggupati, P., George, C., Srinivasan, R., and Arnold, J.: Introducing a new open source GIS user interface for the SWAT model, Environmental modelling & software, 85, 129–138, https://doi.org/10.1016/j.envsoft.2016.08.004, 2016.

Duran-Encalada, J. A., Paucar-Caceres, A., Bandala, E. R., and Wright, G. H.: The impact of global climate change on water quantity and quality: A system dynamics approach to the US–Mexican transborder region, European Journal of Operational Research, 256, 567–581, https://doi.org/10.1016/j.ejor.2016.06.016, 2017.

EEA: CORINE Land Cover 2006 raster data. Version 17 (12/2013), http://www.eea.europa.eu/data-and-maps/data/corine-land-cover-2006-raster-3, 2015.

Efron, B.: Better bootstrap confidence intervals, Journal of the American statistical Association, 82, 171–185, https://doi.org/10.2307/2289144, 1987.

ESRI: ArcGIS Desktop: Release 10.1, 2012.

Euser, T., Winsemius, H. C., Hrachowitz, M., Fenicia, F., Uhlenbrook, S., and Savenije, H. H.: A framework to assess the realism of model structures using hydrological signatures, Hydrology and Earth System Sciences, 17, 1893–1912, https://doi.org/10.5194/hess-17-1893-2013, 2013.

Geoland.at: Digitales Geländemodell (DGM) Österreich, https://www.data.gv.at/katalog/dataset/b5de6975-417b-4320-afdb-eb2a9e2a1dbf, 2015.

Godet, M. and Roubelat, F.: Creating the future : The use and misuse of scenarios, Long Range Planning, 29, 164–171, https://doi.org/10.1016/0024-6301(96)00004-0, 1996.

Gupta, H. and Razavi, S.: Challenges and Future Outlook of Sensitivity Analysis, in: Sensitivity Analysis in Earth Observation Modelling, edited by Petropoulos, G. P. and Srivastava, P. K., chap. 20, pp. 397–415, Elsevier, 1 edn., https://doi.org/10.1016/B978-0-12-803011-0.00020-3, 2017.

Gupta, H. V., Sorooshian, S., and Yapo, P. O.: Status of Automatic Calibration for Hydrologic Models: Comparison with Multilevel Expert Calibration, Journal of Hydrologic Engineering, 4, 135–143, https://doi.org/10.1061/(ASCE)1084-0699(1999)4:2(135), 1999.

Gupta, H. V., Kling, H., Yilmaz, K. K., and Martinez, G. F.: Decomposition of the mean squared error and NSE performance criteria: Implications for improving hydrological modelling, Journal of Hydrology, 377, 80–91, https://doi.org/10.1016/j.jhydrol.2009.08.003, 2009.

Guse, B., Pfannerstill, M., and Fohrer, N.: Dynamic Modelling of Land Use Change Impacts on Nitrate Loads in Rivers, Environmental Processes, 2, 575–592, https://doi.org/10.1007/s40710-015-0099-x, 2015.

5 Guse, B., Pfannerstill, M., Gafurov, A., Fohrer, N., and Gupta, H.: Demasking the integrated information of discharge: Advancing sensitivity analysis to consider different hydrological components and their rates of change, Water Resources Research, 52, 8724–8743, https://doi.org/10.1002/2016WR018894, 2016a.

Guse, B., Pfannerstill, M., Strauch, M., Reusser, D. E., Lüdtke, S., Volk, M., Gupta, H., and Fohrer, N.: On characterizing the temporal dominance patterns of model parameters and processes, Hydrological Processes, 30, 2255–2270, https://doi.org/10.1002/hyp.10764, 2016b.

10 Haas, M. B., Guse, B., Pfannerstill, M., and Fohrer, N.: A joined multi-metric calibration of river discharge and nitrate loads with different performance measures, Journal of Hydrology, 536, 534–545, https://doi.org/10.1016/j.jhydrol.2016.03.001, 2016.

Haghnegahdar, A. and Razavi, S.: Insights into sensitivity analysis of earth and environmental systems models: On the impact of parameter perturbation scale, Environmental Modelling & Software, 95, 115–131, https://doi.org/10.1016/j.envsoft.2017.03.031, 2017.

Haghnegahdar, A., Razavi, S., Yassin, F., and Wheater, H.: Multi-criteria sensitivity analysis as a diagnostic tool for understanding model behavior and characterizing model uncertainty, Hydrological Processes, 31, 4462–4476, https://doi.org/10.1002/hyp.11358, 2017.

15 Haiden, T., Kann, A., Wittmann, C., Pistotnik, G., Bica, B., and Gruber, C.: The Integrated Nowcasting through Comprehensive Analysis (INCA) System and Its Validation over the Eastern Alpine Region, Weather and Forecasting, 26, 166–183, https://doi.org/10.1175/2010WAF2222451.1, 2011.

Hart, J. and Gremaud, P.: Robustness of the Sobol'indices to distributional uncertainty, arXiv preprint arXiv:1803.11249v3, 2018.

20 Hartigan, J. A. and Wong, M. A.: Algorithm AS 136: A K-Means Clustering Algorithm, Applied Statistics, 28, 100, https://doi.org/10.2307/2346830, 1979.

Haslinger, K., Anders, I., and Hofstätter, M.: Regional climate modelling over complex terrain: an evaluation study of COSMO-CLM hindcast model runs for the Greater Alpine Region, Climate Dynamics, 40, 511–529, https://doi.org/10.1007/s00382-012-1452-7, 2013.

Hempel, S., Frieler, K., Warszawski, L., Schewe, J., and Piontek, F.: A trend-preserving bias correction - The ISI-MIP approach, Earth System Dynamics, 4, 219–236, https://doi.org/10.5194/esd-4-219-2013, 2013.

Hengl, T., De Jesus, J. M., Heuvelink, G. B., Gonzalez, M. R., Kilibarda, M., Blagotić, A., Shangguan, W., Wright, M. N., Geng, X., Bauer-Marschallinger, B., Guevara, M. A., Vargas, R., MacMillan, R. A., Batjes, N. H., Leenaars, J. G., Ribeiro, E., Wheeler, I., Mantel, S., and Kempen, B.: SoilGrids250m: Global gridded soil information based on machine learning, PLoS one, 12, 1–40, https://doi.org/10.1371/journal.pone.0169748, 2017.

30 Hiebl, J. and Frei, C.: Daily temperature grids for Austria since 1961—concept, creation and applicability, Theoretical and Applied Climatology, 124, 161–178, https://doi.org/10.1007/s00704-015-1411-4, 2016.

Hinkley, D. V.: Bootstrap methods, Journal of the Royal Statistical Society. Series B (Methodological), pp. 321–337, 1988.

Hofstätter, M., Ganekind, M., and Hiebl, J.: GPARD-6: A new 60-year gridded precipitation dataset for Austria based on daily rain gauge measurements, in: DACH 2013 - Deutsch-Österreichisch-Schweizerische Meteorologen-Tagung, Innsbruck, Austria, 2013.

35 Houska, T., Kraft, P., Chamorro-Chavez, A., and Breuer, L.: SPOTting model parameters using a ready-made python package, PloS one, 10, e0145 180, https://doi.org/10.1371/journal.pone.0145180, 2015.

Hrachowitz, M., Fovet, O., Ruiz, L., Euser, T., Gharari, S., Nijzink, R., Freer, J., Savenije, H. H., and Gascuel-Odoux, C.: Process consistency in models: The importance of system signatures, expert knowledge, and process complexity, Water Resources Research, 50, 7445–7469, https://doi.org/10.1002/2014WR015484, 2014.

Iooss, B., Janon, A., Pujol, G., with contributions from Khalid Boumhaout, Veiga, S. D., Delage, T., Fruth, J., Gilquin, L., Guillaume, J., Le Gratiet, L., Lemaitre, P., Nelson, B. L., Monari, F., Oomen, R., Ramos, B., Roustant, O., Song, E., Staum, J., Sueur, R., Touati, T., and Weber, F.: sensitivity: Global Sensitivity Analysis of Model Outputs, https://CRAN.R-project.org/package=sensitivity, r package version 1.15.1, 2018.

Jacob, D., Petersen, J., Eggert, B., Alias, A., Christensen, O. B., Bouwer, L. M., Braun, A., Colette, A., Déqué, M., Georgievski, G., Georgopoulou, E., Gobiet, A., Menut, L., Nikulin, G., Haensler, A., Hempelmann, N., Jones, C., Keuler, K., Kovats, S., Kröner, N., Kotlarski, S., Kriegsmann, A., Martin, E., van Meijgaard, E., Moseley, C., Pfeifer, S., Preuschmann, S., Radermacher, C., Radtke, K., Rechid, D., Rounsevell, M., Samuelsson, P., Somot, S., Soussana, J.-F., Teichmann, C., Valentini, R., Vautard, R., Weber, B., and Yiou, P.: EURO-CORDEX: new high-resolution climate change projections for European impact research, Regional Environmental Change, 14, 563–578, https://doi.org/10.1007/s10113-013-0499-2, 2014.

Jha, M., Gassman, P. W., Secchi, S., Gu, R., and Arnold, J.: Effect of Watershed Subdivision on SWAT Flow, Sediment, and Nutrient Predictions, Journal of the American Water Resources Association, 40, 811–825, https://doi.org/10.1111/j.1752-1688.2004.tb04460.x, 2004.

Jiménez, B. E., Oki, T., Arnell, N. W., Benito, G., Cogley, J. G., Döll, P., Jiang, T., and Mwakalila, S. S.: Freshwater Resources., in: Climate Change 2014: Impacts, Adaptation, and Vulnerability. Part A: Global and Sectoral Aspects. Contribution of Working Group II to the Fifth Assessment Report of the Intergovernmental Panel on Climate Change, edited by Field, C., Barros, V., Dokken, D., Mach, K., Mastrandrea, M., Bilir, T., Chatterjee, M., Ebi, K., Estrada, Y., Genova, R., Girma, B., Kissel, E., Levy, A., MacCracken, S., Mastrandrea, P., and White, L., pp. 229–269, Cambridge University Press, Cambridge, United Kingdom and New York, NY, USA, 2014.

Jones, R., Patwardhan, A., Cohen, S., Dessai, S., Lammel, A., Lempert, R., Mirza, M., and von Storch, H.: Foundations for Decision Making, in: Climate Change 2014: Impacts, Adaptation, and Vulnerability. Part A: Global and Sectoral Aspects. Contribution of Working Group II to the Fifth Assessment Report of the Intergovernmental Panel on Climate Change, edited by Field, C., Barros, V., Dokken, D., Mach, K., Mastrandrea, M., Bilir, T., Chatterjee, M., Ebi, K., Estrada, Y., Genova, R., Girma, B., Kissel, E., Levy, A., MacCracken, S., Mastrandrea, P., and White, L., pp. 195–228, Cambridge University Press, Cambridge, United Kingdom and New York, NY, USA, https://doi.org/10.1017/CBO9781107415379.007, 2014.

Knutti, R. and Sedláček, J.: Robustness and uncertainties in the new CMIP5 climate model projections, Nature Climate Change, 3, 369–373, https://doi.org/10.1038/nclimate1716, 2013.

Land NÖ: Landwirtschaftliche Bildung in NÖ - Versuche, http://www.lako.at/de/versuche/?lang=de{&}a=179{&}a{_}urlname=versuche{&}versuche{_}a=1, 2015.

LGBl. Nr. 39/2015: Verordnung des Landeshauptmannes von Steiermark vom 20. Mai 2015, mit der ein Regionalprogramm zum Schutz der Grundwasserkörper Grazer Feld, Leibnitzer Feld und Unteres Murtal erlassen und Schongebiete bestimmt werden (Grundwasserschutzprogramm Graz bis B, 2015.

Mahmoud, M., Liu, Y., Hartmann, H., Stewart, S., Wagener, T., Semmens, D., Stewart, R., Gupta, H., Dominguez, D., Dominguez, F., Hulse, D., Letcher, R., Rashleigh, B., Smith, C., Street, R., Ticehurst, J., Twery, M., van Delden, H., Waldick, R., White, D., and Winter, L.: A formal framework for scenario development in support of environmental decision-making, Environmental Modelling and Software, 24, 798–808, https://doi.org/10.1016/j.envsoft.2008.11.010, 2009.

Mara, T. A. and Tarantola, S.: Variance-based sensitivity indices for models with dependent inputs, Reliability Engineering & System Safety, 107, 115–121, https://doi.org/10.1016/j.ress.2011.08.008, 2012.

Massmann, C. and Holzmann, H.: Analysing the Sub-processes of a Conceptual Rainfall-Runoff Model Using Information About the Parameter Sensitivity and Variance, Environmental Modeling and Assessment, 20, 41–53, https://doi.org/10.1007/s10666-014-9414-6, 2015.

5 Massmann, C., Wagener, T., and Holzmann, H.: A new approach to visualizing time-varying sensitivity indices for environmental model diagnostics across evaluation time-scales, Environmental Modelling & Software, 51, 190–194, https://doi.org/10.1016/J.ENVSOFT.2013.09.033, 2014.

Mehdi, B., Lehner, B., Gombault, C., Michaud, A., Beaudin, I., Sottile, M.-F., and Blondlot, A.: Simulated impacts of climate change and agricultural land use change on surface water quality with and without adaptation management strategies, Agriculture, Ecosystems & Environment, 213, 47–60, https://doi.org/10.1016/j.agee.2015.07.019, 2015a.

Mehdi, B., Ludwig, R., and Lehner, B.: Evaluating the impacts of climate change and crop land use change on streamflow, nitrates and phosphorus: A modeling study in Bavaria, Journal of Hydrology: Regional Studies, 4, 60–90, https://doi.org/10.1016/j.ejrh.2015.04.009, 2015b.

Mehdi, B., Schulz, K., Ludwig, R., Ferber, F., and Lehner, B.: Evaluating the Importance of Non-Unique Behavioural Parameter Sets on Surface Water Quality Variables under Climate Change Conditions in a Mesoscale Agricultural Watershed, Water Resources Management, 32, 619–639, https://doi.org/10.1007/s11269-017-1830-3, 2018.

Milly, P. C. D. and Dunne, K. A.: On the hydrologic adjustment of climate-model projections: The potential pitfall of potential evapotranspiration, Earth Interactions, 15, 1–14, https://doi.org/10.1175/2010EI363.1, 2011.

Milly, P. C. D., Betancourt, J., Falkenmark, M., Hirsch, R. M., Kundzewicz, Z. W., Lettenmaier, D. P., and Stouffer, R. J.: Climate change. Stationarity is dead: whither water management?, Science, 319, 573–574, https://doi.org/10.1126/science.1151915, 2008.

Momm, H. G., Bingner, R. L., Emilaire, R., Garbrecht, J., Wells, R. R., and Kuhnle, R. A.: Automated watershed subdivision for simulations using multi-objective optimization, Hydrological Sciences Journal, 62, 1564–1582, https://doi.org/10.1080/02626667.2017.1346794, 2017.

Moriasi, D., Arnold, J., Van Liew, M., Binger, R., Harmel, R., and Veith, T.: Model evaluation guidelines for systematic quantification of accuracy in watershed simulations, Transactions of the ASABE, 50, 885–900, https://doi.org/10.13031/2013.23153, 2007.

Morris, M. D.: Factorial sampling plans for preliminary computational experiments, Technometrics, 33, 161–174, 1991.

Moss, R. H., Edmonds, J. A., Hibbard, K. A., Manning, M. R., Rose, S. K., Van Vuuren, D. P., Carter, T. R., Emori, S., Kainuma, M., Kram, T., Meehl, G. A., Mitchell, J. F., Nakicenovic, N., Riahi, K., Smith, S. J., Stouffer, R. J., Thomson, A. M., Weyant, J. P., and Wilbanks, T. J.: The next generation of scenarios for climate change research and assessment, Nature, 463, 747–756, https://doi.org/10.1038/nature08823, 2010.

Muerth, M. J., Gauvin St-Denis, B., Ricard, S., Velázquez, J. A., Schmid, J., Minville, M., Caya, D., Chaumont, D., Ludwig, R., and Turcotte, R.: On the need for bias correction in regional climate scenarios to assess climate change impacts on river runoff, Hydrology and Earth System Sciences, 17, 1189–1204, https://doi.org/10.5194/hess-17-1189-2013, 2013.

Nash, J. E. and Sutcliffe, J. V.: River flow forecasting through conceptual models part I - A discussion of principles, Journal of Hydrology, 10, 282–290, https://doi.org/10.1016/0022-1694(70)90255-6, 1970.

Neitsch, S., Arnold, J., Kiniry, J., and Williams, J.: Soil and Water Assessment Tool Theoretical Documentation Version 2009, Tech. rep., Texas Water Resources Institute, Temple, Texas, 2011.

ÖWAV: ÖWAV-Regelblatt 25: Abwasserentsorgung in dünn besiedelten Gebieten, 2. vollständig überarbeitete Auflage, 2010.

Pfannerstill, M., Guse, B., and Fohrer, N.: Smart low flow signature metrics for an improved overall performance evaluation of hydrological models, Journal of Hydrology, 510, 447–458, https://doi.org/10.1016/j.jhydrol.2013.12.044, 2014.

Pfannerstill, M., Bieger, K., Guse, B., Bosch, D. D., Fohrer, N., and Arnold, J. G.: How to Constrain Multi-Objective Calibrations of the SWAT Model Using Water Balance Components, Journal of the American Water Resources Association, 53, 532–546, https://doi.org/10.1111/1752-1688.12524, 2017.

Pianosi, F. and Wagener, T.: A simple and efficient method for global sensitivity analysis based on cumulative distribution functions, Environmental Modelling & Software, 67, 1–11, https://doi.org/10.1016/j.envsoft.2015.01.004, 2015.

Pianosi, F. and Wagener, T.: Distribution-based sensitivity analysis from a generic input-output sample, Environmental Modelling & Software, 108, 197–207, https://doi.org/10.1016/j.envsoft.2018.07.019, 2018.

Pianosi, F., Beven, K., Freer, J., Hall, J. W., Rougier, J., Stephenson, D. B., and Wagener, T.: Sensitivity analysis of environmental models: A systematic review with practical workflow, Environmental Modelling & Software, 79, 214–232, https://doi.org/10.1016/j.envsoft.2016.02.008, 2016.

Pignotti, G., Rathjens, H., Cibin, R., Chaubey, I., and Crawford, M.: Comparative analysis of HRU and grid-based SWAT models, Water, 9, 272, https://doi.org/10.3390/w9040272, 2017.

R Core Team: R: A language and environment for statistical computing., https://www.r-project.org/, 2017.

Rakovec, O., Hill, M. C., Clark, M. P., Weerts, A. H., Teuling, A. J., and Uijlenhoet, R.: Distributed Evaluation of Local Sensitivity Analysis (DELSA), with application to hydrologic models, Water Resour. Res, 50, 409–426, https://doi.org/10.1002/2013WR014063, 2014.

Razavi, S. and Gupta, H. V.: What do we mean by sensitivity analysis? The need for comprehensive characterization of "global" sensitivity in Earth and Environmental systems models, Water Resources Research, 51, 3070–3092, https://doi.org/10.1002/2014WR016527, 2015.

Razavi, S. and Gupta, H. V.: A new framework for comprehensive, robust, and efficient global sensitivity analysis: 1. Theory, Water Resources Research, 52, 423–439, https://doi.org/10.1002/2015WR017558, 2016a.

Razavi, S. and Gupta, H. V.: A new framework for comprehensive, robust, and efficient global sensitivity analysis: 2. Application, Water Resources Research, 52, 440–455, https://doi.org/10.1002/2015WR017559, 2016b.

Reusser, D.: fast: Implementation of the Fourier Amplitude Sensitivity Test (FAST), https://CRAN.R-project.org/package=fast, r package version 0.64, 2015.

Riahi, K., Grübler, A., and Nakicenovic, N.: Scenarios of long-term socio-economic and environmental development under climate stabilization, Technological Forecasting and Social Change, 74, 887–935, https://doi.org/10.1016/j.techfore.2006.05.026, 2007.

Roderick, M. L., Sun, F., Lim, W. H., and Farquhar, G. D.: A general framework for understanding the response of the water cycle to global warming over land and ocean, Hydrology and Earth System Sciences, 18, 1575–1589, https://doi.org/10.5194/hess-18-1575-2014, 2014.

Rosolem, R., Gupta, H. V., Shuttleworth, W. J., Zeng, X., and De Gonçalves, L. G. G.: A fully multiple-criteria implementation of the Sobol method for parameter sensitivity analysis, Journal of Geophysical Research: Atmospheres, 117, https://doi.org/10.1029/2011JD016355, 2012.

Rounsevell, M. D. and Metzger, M. J.: Developing qualitative scenario storylines for environmental change assessment, https://doi.org/10.1002/wcc.63, 2010.

Ruzicka, K., Gabriel, O., Bletterie, U., Winkler, S., and Zessner, M.: Cause and effect relationship between foam formation and treated wastewater effluents in a transboundary river, Physics and Chemistry of the Earth, 34, 565–573, https://doi.org/10.1016/j.pce.2009.01.002, 2009.

Saltelli, A. and Annoni, P.: How to avoid a perfunctory sensitivity analysis, Environmental Modelling & Software, 25, 1508–1517, https://doi.org/10.1016/j.envsoft.2010.04.012, 2010.

Saltelli, A. and Tarantola, S.: On the Relative Importance of Input Factors in Mathematical Models, Journal of the American Statistical Association, 97, 702–709, https://doi.org/10.1198/016214502388618447, 2002.

5 Saltelli, A., Tarantola, S., Campolongo, F., and Ratto, M.: Sensitivity analysis in practice: A guide to assessing scientific models, vol. 91, John Wiley & Sons Ltd, Chichester, West Sussex, UK, 1 edn., 2004.

Saltelli, A., Ratto, M., Andres, T., Campolongo, F., Cariboni, J., Gatelli, D., Saisana, M., and Tarantola, S.: Global Sensitivity Analysis. The Primer, John Wiley & Sons, Ltd, Chichester, UK, https://doi.org/10.1002/9780470725184, 2008.

Sarrazin, F., Pianosi, F., and Wagener, T.: Global Sensitivity Analysis of environmental models: Convergence and validation, Environmental
10 Modelling & Software, 79, 135–152, https://doi.org/10.1016/j.envsoft.2016.02.005, 2016.

Savage, J. T. S., Pianosi, F., Bates, P., Freer, J., and Wagener, T.: Quantifying the importance of spatial resolution and other factors through global sensitivity analysis of a flood inundation model, Water Resources Research, 52, 9146–9163, https://doi.org/10.1002/2015WR018198, 2016.

Schönhart, M., Trautvetter, H., Parajka, J., Blaschke, A. P., Hepp, G., Kirchner, M., Mitter, H., Schmid, E., Strenn, B., and Zess-
15 ner, M.: Modelled impacts of policies and climate change on land use and water quality in Austria, Land Use Policy, 76, 500–514, https://doi.org/10.1016/j.landusepol.2018.02.031, 2018.

Schulz, K., Beven, K., and Huwe, B.: Equifinality and the problem of robust calibration in nitrogen budget simulations, Soil Science Society of America Journal, 63, 1934–1941, https://doi.org/10.2136/sssaj1999.6361934x, 1999.

Shaw, S. B. and Riha, S. J.: Assessing temperature-based PET equations under a changing climate in temperate, deciduous forests, Hydro-
20 logical Processes, 25, 1466–1478, https://doi.org/10.1002/hyp.7913, 2011.

Sheffield, J., Wood, E. F., and Roderick, M. L.: Little change in global drought over the past 60 years, Nature, 491, 435–438, https://doi.org/10.1038/nature11575, 2012.

Sheikholeslami, R., Razavi, S., Gupta, H. V., Becker, W., and Haghnegahdar, A.: Global sensitivity analysis for high-dimensional problems: How to objectively group factors and measure robustness and convergence while reducing computational cost, Environmental Modelling
25 & Software, 111, 282–299, https://doi.org/doi.org/10.1016/j.envsoft.2018.09.002, 2019.

Smith, S. J. and Wigley, T. M.: Multi-gas forcing stabilization with minicam, Energy Journal, 27, 373–391, https://doi.org/10.5547/ISSN0195-6574-EJ-VolSI2006-NoSI3-19, 2006.

Sobol, I. M.: Sensitivity analysis for nonlinear mathematical models, Mathematical Modelling and Computational Experiments, 4, 407–414, https://doi.org/10.18287/0134-2452-2015-39-4-459-461., 1993.

30 Statistik Austria: ÖROK-Regionalprognosen 2014 - Bevölkerung, Ausführliche Tabellen zur kleinräumigen ÖROK-Prognose 2014, http://www.oerok.gv.at/, 2015a.

Statistik Austria: STATCube - Statistical Data base of the Statistik Austria: Agricultural census - Land use (not openly accessible), http://statcube.at/statistik.at/ext/statcube, 2015b.

Statistik Austria: Datenbank zur Bevölkerungsprognose 2016 - Hauptszenario, https://www.statistik.at/, 2016.

35 Statistik Austria: STATCube - Statistical Data base of the Statistik Austria: Agricultural and forestry holdings with arable land and their cultivated land area (not openly accessible), data.http://statcube.at/statistik.at/ext/statcube, 2017.

Strauch, M., Schweppe, R., and Schürz, C.: TopHRU: Threshold optimization for HRUs in SWAT, https://doi.org/10.5281/zenodo.154379, https://github.com/michstrauch/TopHRU/tree/v1.2, 2016.

Tarantola, S. and Mara, T. A.: Variance-based sensitivity indices of computer models with dependent inputs: The Fourier Amplitude Sensitivity Test, International Journal for Uncertainty Quantification, 7, https://doi.org/10.1615/Int.J.UncertaintyQuantification.2017020291, 2017.

Teutschbein, C. and Seibert, J.: Bias correction of regional climate model simulations for hydrological climate-change impact studies: Review and evaluation of different methods, Journal of Hydrology, 456-457, 12–29, https://doi.org/10.1016/j.jhydrol.2012.05.052, 2012.

Teutschbein, C. and Seibert, J.: Is bias correction of regional climate model (RCM) simulations possible for non-stationary conditions, Hydrology and Earth System Sciences, 17, 5061–5077, https://doi.org/10.5194/hess-17-5061-2013, 2013.

Tóth, B., Weynants, M., Nemes, A., Makó, A., Bilas, G., and Tóth, G.: New generation of hydraulic pedotransfer functions for Europe, European Journal of Soil Science, 66, 226–238, https://doi.org/10.1111/ejss.12192, 2015.

Tripathi, M. P., Raghuwanshi, N. S., and Rao, G. P.: Effect of watershed subdivision on simulation of water balance components, Hydrological Processes, 20, 1137–1156, https://doi.org/10.1002/hyp.5927, 2006.

van Vuuren, D. P., Edmonds, J., Kainuma, M., Riahi, K., Thomson, A., Hibbard, K., Hurtt, G. C., Kram, T., Krey, V., Lamarque, J. F., Masui, T., Meinshausen, M., Nakicenovic, N., Smith, S. J., and Rose, S. K.: The representative concentration pathways: An overview, Climatic Change, 109, 5–31, https://doi.org/10.1007/s10584-011-0148-z, 2011.

van Vuuren, D. P., Kok, M. T., Girod, B., Lucas, P. L., and de Vries, B.: Scenarios in Global Environmental Assessments: Key characteristics and lessons for future use, Global Environmental Change, 22, 884–895, https://doi.org/10.1016/j.gloenvcha.2012.06.001, 2012.

Wagner, P. D., Bhallamudi, S. M., Narasimhan, B., Kumar, S., Fohrer, N., and Fiener, P.: Comparing the effects of dynamic versus static representations of land use change in hydrologic impact assessments, Environmental Modelling and Software, pp. 1–9, https://doi.org/10.1016/j.envsoft.2017.06.023, 2017.

Wilby, R. L.: Uncertainty in water resource model parameters used for climate change impact assessment, Hydrological Processes, 19, 3201–3219, https://doi.org/10.1002/hyp.5819, 2005.

Wilby, R. L., Wigley, T. M. L., Conway, D., Jones, P. D., Hewitson, B. C., Main, J., and Wilks, D. S.: Statistical downscaling of general circulation model output: A comparison of methods, Water Resour. Res., 34, 2995–3008, https://doi.org/10.1029/98wr02577, 1998.

Willmott, C. J., Robeson, S. M., and Matsuura, K.: A refined index of model performance, International Journal of Climatology, 32, 2088–2094, https://doi.org/10.1002/joc.2419, 2012.

Winchell, M., Srinivasan, R., Di Luzio, M., and Arnold, J. G.: ArcSWAT 2012.10.19 Interface for SWAT2012, http://swat.tamu.edu/software/arcswat/, 2015.

Wise, M., Calvin, K., Thomson, A., Clarke, L., Bond-Lamberty, B., Sands, R., Smith, S. J., Janetos, A., and Edmonds, J.: Implications of Limiting CO2 Concentrations for Land Use and Energy, Science, 324, 1183–1186, https://doi.org/10.1126/science.1168475, 2009.

Wood, A. W., Leung, L. R., Sridhar, V., and Lettenmaier, D. P.: Hydrologic implications of dynamical and statistical approaches to downscaling climate model outputs, Climatic Change, 62, 189–216, https://doi.org/10.1023/B:CLIM.0000013685.99609.9e, 2004.

Yates, D. N., Miller, K. A., Wilby, R. L., and Kaatz, L.: Decision-centric adaptation appraisal for water management across Colorado's Continental Divide, Climate Risk Management, 10, 35–50, https://doi.org/10.1016/j.crm.2015.06.001, 2015.

Zadeh, F. K., Nossent, J., Sarrazin, F., Pianosi, F., van Griensven, A., Wagener, T., and Bauwens, W.: Comparison of variance-based and moment-independent global sensitivity analysis approaches by application to the SWAT model, Environmental Modelling and Software, 91, 210–222, https://doi.org/10.1016/j.envsoft.2017.02.001, 2017.

Zorita, E. and Von Storch, H.: The analog method as a simple statistical downscaling technique: Comparison with more complicated methods, Journal of Climate, 12, 2474–2489, https://doi.org/10.1175/1520-0442(1999)012<2474:TAMAAS>2.0.CO;2, 1999.